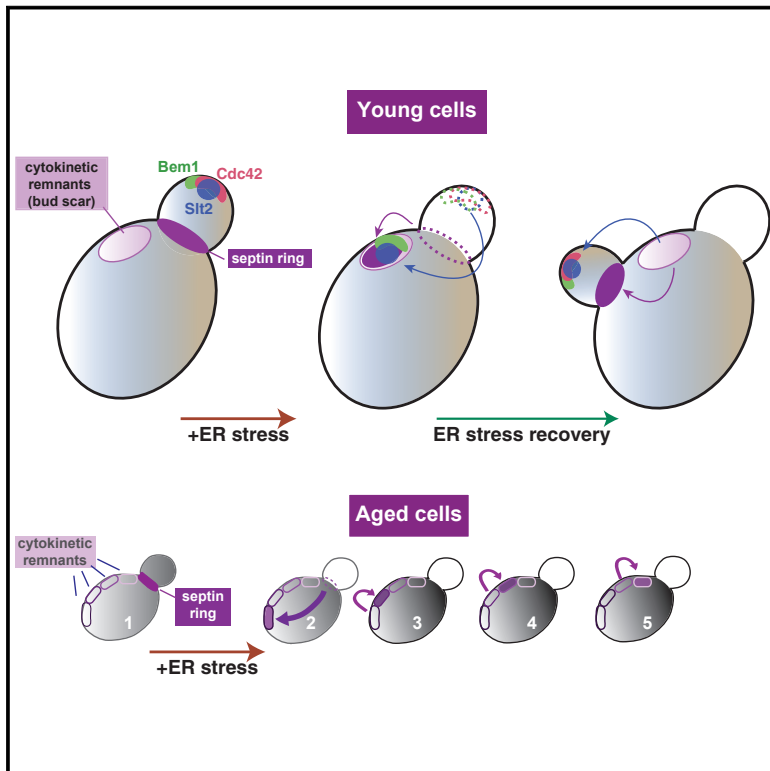


# Developmental Cell

## Transfer of the Septin Ring to Cytokinetic Remnants in ER Stress Directs Age-Sensitive Cell-Cycle Re-entry

### Graphical Abstract



### Authors

Jesse T. Chao, Francisco Piña, Masayuki Onishi, Yifat Cohen, Ya-Shiuan Lai, Maya Schuldiner, Maho Niwa

### Correspondence

mniwarosen@ucsd.edu

### In Brief

How cells manage a sudden onset of stress is crucial for their survival. Chao et al. show that cells under ER stress can temporarily pause the cell cycle until the stress is mitigated. They accomplish this by transferring cell polarity components away from growth sites and onto cytokinetic remnants.

### Highlights

- The septin ring transfer from the bud neck to the bud scar is an ERSU holmark event in response to ER stress
- Transfer of the septin ring is required for timely re-entry into the cell cycle
- Slit2 inactivates Cdc42 and is essential for cell survival under ER stress
- Age impacts cell-cycle re-entry upon ER stress recovery

# Transfer of the Septin Ring to Cytokinetic Remnants in ER Stress Directs Age-Sensitive Cell-Cycle Re-entry

Jesse T. Chao,<sup>1</sup> Francisco Piña,<sup>1</sup> Masayuki Onishi,<sup>2,4</sup> Yifat Cohen,<sup>3,4</sup> Ya-Shiuan Lai,<sup>1</sup> Maya Schuldiner,<sup>3</sup> and Maho Niwa<sup>1,5,\*</sup>

<sup>1</sup>Division of Biological Sciences, Section of Molecular Biology, University of California, San Diego, La Jolla, CA 92093-0377, USA

<sup>2</sup>Department of Genetics, Stanford University School of Medicine, Stanford, CA 94305-5120, USA

<sup>3</sup>Department of Molecular Genetics, Weizmann Institute of Science, Rehovot 7610001, Israel

<sup>4</sup>These authors contributed equally

<sup>5</sup>Lead Contact

\*Correspondence: [mniwarosen@ucsd.edu](mailto:mniwarosen@ucsd.edu)

<https://doi.org/10.1016/j.devcel.2019.08.017>

## SUMMARY

During cell division, the inheritance of a functional endoplasmic reticulum (ER) is ensured by the endoplasmic reticulum stress surveillance (ERSU) pathway. Activation of ERSU causes the septin ring to mislocalize, which blocks ER inheritance and cytokinesis. Here, we uncover that the septin ring in fact translocates to previously utilized cell division sites called cytokinetic remnants (CRMs). This unconventional translocation requires Nba1, a negative polarity regulator that normally prevents repolarization and re-budding at CRMs. Furthermore, septin ring translocation relies on the recruitment and activation of a key ERSU component Slt2 by Bem1, without activating Cdc42. Failure to transfer all septin subunits to CRMs delays the cell's ability to re-enter the cell cycle when ER homeostasis is restored and hinders cell growth after ER stress recovery. Thus, these deliberate but unprecedented rearrangements of cell polarity factors during ER stress safeguard cell survival and the timely cell-cycle re-entry upon ER stress recovery.

## INTRODUCTION

The functions of eukaryotic cells are organized and distributed into specific organelles. During the cell cycle, not only does the genome divide but organelles must be correctly distributed. Thus, one of the fundamental questions in cell biology is how specific organelles are inherited during the cell cycle. The endoplasmic reticulum (ER) is the major organelle responsible for the production and quality control of almost all secretory proteins. In addition, the ER is crucial for lipid biosynthesis and calcium homeostasis (Denic et al., 2006; Feige and Hendershot, 2011; Frakes and Dillin, 2017; Mori, 2000; Ron and Walter, 2007; Rutkowski and Kaufman, 2004). Importantly, the ER cannot be synthesized *de novo* and, instead, must be inherited

from the mother cell. This suggests the presence of ER inheritance checkpoints.

The budding yeast, *Saccharomyces cerevisiae*, is an ideal model organism to study the division of the ER during the cell cycle, due to the asymmetric nature of yeast cell division. The ER in yeast is spatially segregated into the cortical ER (cER) that lies in the cell cortex, with some sections of the cER contacting the plasma membrane. The cER is connected by a few ER tubules with the peri-nuclear ER that is contiguous with the outer nuclear envelope (Westrate et al., 2015; Barlowe, 2010; Bechmann et al., 2012; Du et al., 2004; Fehrenbacher et al., 2002; Hereford and Hartwell, 1974).

Previously, we discovered a cell-cycle checkpoint for ensuring that functional ER is transferred to the daughter cell during the cell cycle, which we termed the ER stress surveillance (ERSU) pathway (Babour et al., 2010; Piña et al., 2016, 2018; Piña and Niwa, 2015). If the accumulation of unfolded or misfolded proteins exceeds ER functional capacity, ER homeostasis is disrupted, leading to a condition known as ER stress. In response to ER stress during the cell cycle, the ERSU pathway blocks the inheritance of the “stressed ER” into the daughter cell and mobilizes the septin ring from the bud neck, ultimately leading to cell-cycle arrest at cytokinesis.

Surprisingly, the ERSU is independent of the well-known unfolded protein response (UPR) signaling pathway that regulates ER functional homeostasis. In parallel to the ERSU pathway, ER stress activates the UPR pathway to up-regulate the transcription of genes coding for ER chaperones and protein folding components to re-establish ER functional homeostasis (Ron and Walter, 2007). When ER functional homeostasis is re-established, cells are released from cell-cycle arrest, re-enter the cell cycle, and inherit a functional ER into the daughter cell (Babour et al., 2010). Thus, the ERSU is one of the checkpoint mechanisms, and works in concert with the UPR pathway to ensure proper organelle inheritance.

One of the hallmark events of ERSU is septin ring mislocalization away from the bud neck. This process is a key mechanism leading to cytokinesis arrest in response to ER stress. The septin ring is composed of five septin subunits, Shs1, Cdc3, 10, 11, and 12, and its formation is dynamically regulated during the cell cycle (Field and Kellogg, 1999; Gladfelter et al., 2001;

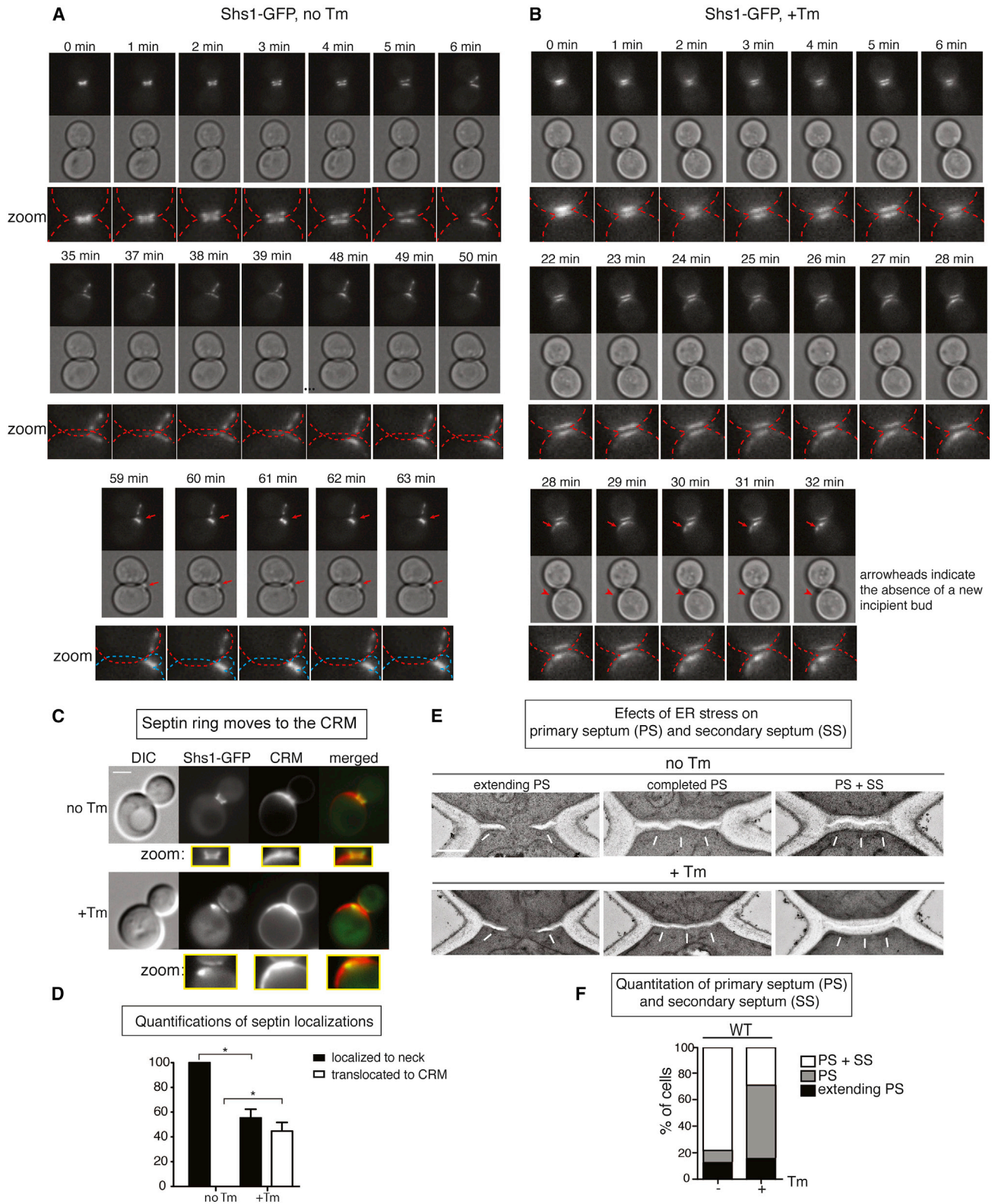


**Figure 1. Septin Rings Relocalize to CRMs during ER Stress**

(A) Time-lapse analysis of septin dynamics (Shs1-GFP) in untreated WT cells. All scale bars, 2  $\mu$ m. Later in the time course, a newly formed septin ring and a daughter cell are indicated by red arrows. Zoom up pictures of bud necks. Related to [Video S1](#).

(legend continued on next page)

Mostowy and Cossart, 2012; Oh and Bi, 2011; Versele and Thorner, 2005; Weirich et al., 2008). Septin ring formation occurs even prior to the emergence of the daughter cell (bud), marking the incipient bud site. The formation of the septin ring is tightly linked to the targeting of activated Cdc42, which allows emergence and polarized growth of the bud. Cdc42 activity is tightly regulated by its upstream components including Cdc24, a GTP exchange factor (GEF) of Cdc42, and Bud1/Rsr1. The septin ring stays at the bud neck between the mother and daughter cells throughout most of the cell cycle. At the end of the cell cycle, the dividing membrane between the mother and daughter cell (i.e., the septum) forms, followed by cell division. Finally, the septin ring disassembles into subunits, which then re-initiate the cycle of assembly and disassembly. Interestingly, septin ring assembly is normally inhibited at cytokinesis remnants (CRMs), which are previously utilized cell-cycle division sites, through a block involving Nba1 (Meitinger et al., 2014). This ensures that budding and subsequent cytokinesis occurs only at naïve locations that have never been used as cell division sites. The number of CRMs increases as a yeast cell undergoes more rounds of cell cycle, and thus it provides a molecular clock for the age of the yeast cell (Caudron and Barral, 2009).

Septin ring mislocalization is important for the ERSU pathway. In *slt2Δ* cells that are unable to mount the ERSU response, the septin ring remains present at the bud neck during ER stress and cells subsequently die. However, we still do not know the details of how septin rings become mislocalized, or the functional significance of this process. Therefore, in this study we used molecular and cell biology approaches to investigate septin ring dynamics during ER stress.

## RESULTS

### The Septin Ring Moves to the Bud Scar in Response to ER Stress

To characterize septin ring movement during ER stress, we performed time-lapse microscopy. We monitored the morphology and localization of the septin ring in a wild-type (WT) cell carrying green fluorescent protein (GFP)-tagged septin subunit Shs1 (Shs1-GFP). Previously, we found that the formation of septin rings occurred normally at the bud neck in small budded cells even under ER-stressed conditions (Babour et al., 2010). Thus, we reasoned that any mislocalization of the septin ring must occur at a later cell-cycle stage and monitored the behavior of Shs1-GFP in large budded G2 cells. Under normal growth, as cells entered mitosis, the Shs1-GFP ring split into two and its fluorescent levels started to decrease. Subsequently, Shs1-GFP began to accumulate at the incipient bud site (Figure 1A; Video S1), consistent with previously reported

septin ring dynamics (Oh and Bi, 2011; Versele and Thorner, 2005).

To monitor Shs1-GFP dynamics under ER stress, we switched to growth medium containing tunicamycin (Tm), a well-characterized ER stress inducer. Tm inhibits protein N-glycosylation in the ER, resulting in an accumulation of unfolded proteins (Kuo and Lampen, 1974). In marked contrast to cells grown in normal media, the septin ring moved to a site adjacent to the bud neck (Figure 1B; Video S2). Importantly, we observed no apical growth of a new daughter cell at the site of septin translocation (Video S2).

In the BY genetic background, haploid cells adopt an axial budding pattern in which new buds consistently form adjacent to the previous bud site or CRMs that include both bud and birth scars. We found that under ER stress, ~45% of Shs1-GFP co-localized with CRMs which could be visualized by calcofluor white (CW) staining (Figures 1C and 1D).

Septin translocation to CRMs was not specific to Tm, as we observed similar Shs1 behavior when we activated ER stress using *ero1-1* temperature-sensitive mutant cells at the non-permissive temperature (Figure S1A) (*ERO1* codes for the oxidoreductase that catalyzes disulfide bond formation in the ER. *ero1-1* at 37°C reliably induces the ER stress response [Frand and Kaiser, 1998; Pollard et al., 1998; Tu et al., 2000]). Previously, we reported that septin subunits, Shs1, Cdc10, 12, and 11 were all mislocalized from the bud neck under ER stress (Babour et al., 2010). Consistently, we saw the co-localization other septin subunits such as Cdc11-GFP and Cdc10-GFP with CRMs (Figures S1B and S3D, respectively). In the W303 yeast strain, new buds emerge from distal positions with respect to the current site of division, presumably due to *BUD4* mutations (Voth et al., 2005). Indeed, we found that Shs1-GFP in W303 background was also localized to CRMs in response to ER stress (Figures S1C–S1E; Videos S3 and S4), revealing that the septin ring translocation to CRMs occurs regardless of which budding pattern was being used.

### Septin Transfer Correlates with Cytokinesis Block during ER Stress

As the septin ring is coordinated with cytokinesis and the formation of primary and secondary septum, which are cell walls that form in between mother and daughter cells (Onishi et al., 2013; Schmidt et al., 2002; Weiss, 2012; Wloka and Bi, 2012), we hypothesized that the translocation of the septin ring might disrupt septum formation. Electron microscopy analyses of both primary and secondary septum revealed that many ER-stressed cells had no secondary septum even though primary septum formed normally (Figures 1E and 1F). We also examined Myo1, which is a type II myosin that forms an actomyosin

(B) Time-lapse analysis of septin rings in WT cells that were treated with 1 μg/mL Tm. Red arrows point to translocated septin rings without the emergence of a new bud that is indicated by red arrowheads. Related to Video S2.

(C) Shs1-GFP cells were grown with (+) or without (–) 1 μg/mL Tm. CRMs were visualized by CW staining. Inserts contain zoomed images from the bud neck region.

(D) Quantifications for Shs1-GFP localization in +/- Tm conditions. \* indicates  $p < 0.001$ .

(E) Representative electron micrographs taken from the bud neck regions of WT cells. Cells were synchronized for 30 min with alpha factor, released and either treated with DMSO (no Tm) or incubated with 15 μg/ml Tm for 2 h (+Tm), and then fixed. White arrows indicate septums; scale bar represents 0.5 μm. PS, primary septum; SS, secondary septum.

(F) Quantification of the experiment in (E). Upon ER stress induction by Tm treatment, the number of cells with primary septum (PS) (but not secondary septum [SS]) (shown in gray) significantly increased. In contrast, both PS and SS formed in unstressed cells (white column).

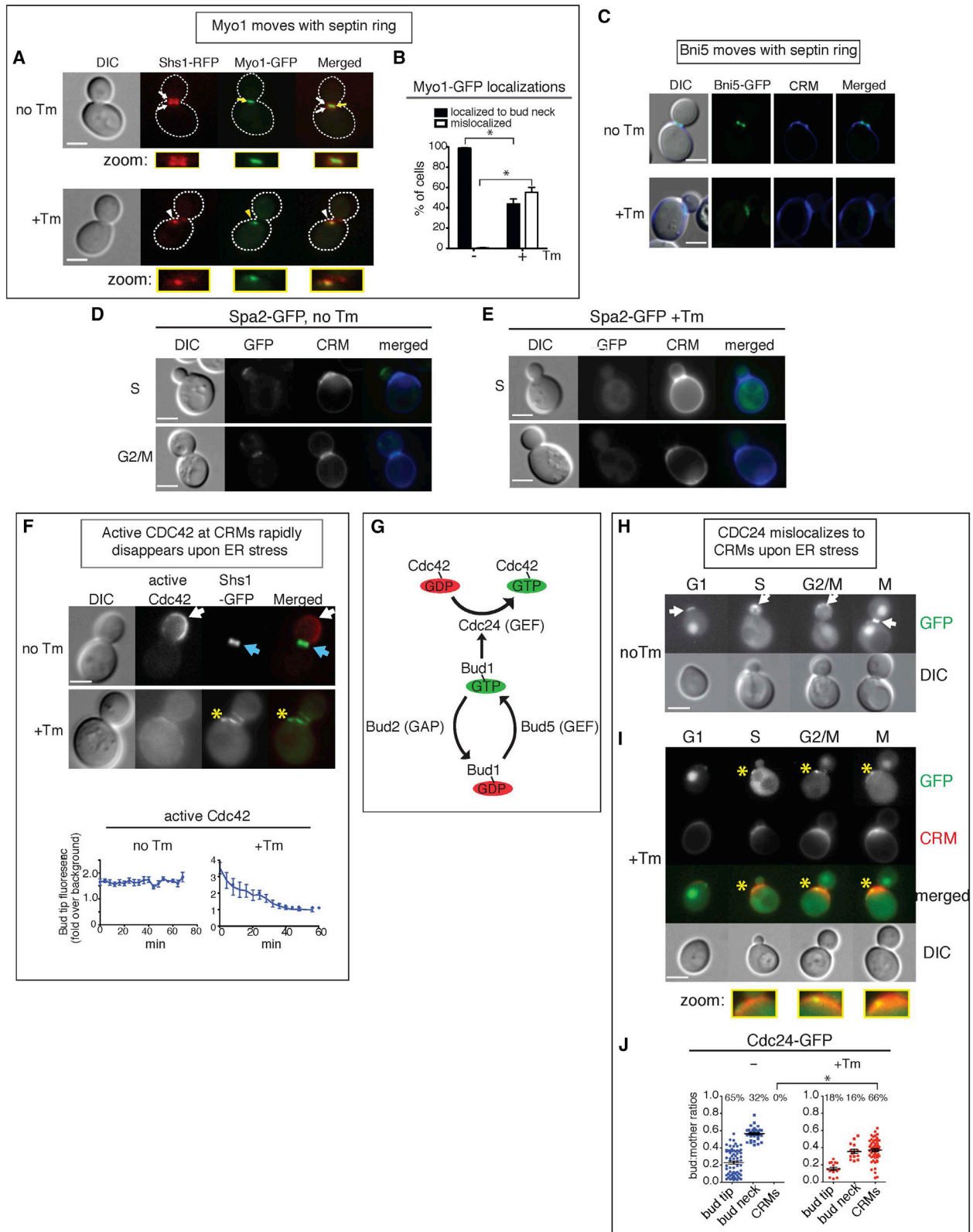


**Figure 2. The Bud1/Rsr1 GTPase Complex Is Negatively Regulated during ER Stress**

(A) Myo1-GFP was co-localized with Shs1-RFP under both normal growth and ER stress. Cells were either grown without or with 1  $\mu$ g/ml Tm. White arrows, RFP localization; yellow arrows, GFP. White and yellow arrowheads show altered localizations of Shs1 and Myo1, respectively. All scale bars, 2  $\mu$ m.

(legend continued on next page)

contractile ring targeted to the bud neck by septins to form the actomyosin contractile ring (Bi et al., 1998; Lippincott and Li, 1998; Tolliday et al., 2003). In unstressed WT cells carrying the genomic replacement of Myo1-GFP and Shs1-RFP, Myo1-GFP was localized at the bud neck and sandwiched between two septin rings (Figure 2A). Upon ER stress induction, Myo1-GFP co-localized with translocated Shs1-RFP, and thus was no longer in the bud neck (Figures 2A and 2B). The Myo1 recruiter, Bni5, also translocated to CRMs as well (Figure 2C). Taken together, these findings suggested that ER stress-induced septin movement occurred concurrently with the mislocalization of the actomyosin contractile ring, leading to a delay in cytokinesis. Curiously, *MYO1* deletion results in multi-budded cells due to defects in cell division despite continued polarized growth (Bi et al., 1998; Lord et al., 2005; Watts et al., 1987). However, the growth phenotype of ER-stressed cells differs from that of *myo1Δ* cells, suggesting that polarized growth is terminated in ER-stressed cells.

### Septin Movement to CRMs Occurs without Induction of Polarized Growth

Our finding that the septin ring translocated to CRMs during ER stress could partially explain the differences in phenotypes between *myo1Δ* cells and ER-stressed cells. Under normal growth, septin ring formation at the presumptive bud site is directed by the master regulator of cell polarity, Cdc42 (Okada et al., 2013). However, at CRMs, a Cdc42-inhibitory circuit is present to prevent “refractory budding” (Meitinger et al., 2014). Thus, translocation to CRMs during ER stress should allow septin ring to access the inactivation mechanism of Cdc42 and polarized growth at CRMs.

To confirm the status of polarized growth in ER stress, we first visualized the polarisome component Spa2, which acts to organize the actin cytoskeleton at sites of polarized growth (Sheu et al., 1998). Spa2 was dispersed and not enriched at CRMs in ER-stressed cells, supporting the lack of the polarized growth (Figures 2D and 2E). A fluorescence biosensor, Gic2-PBD-RFP, visualizes only the active, GTP-bound form of Cdc42 (Okada et al., 2013). In unstressed cells, active Cdc42 was enriched in the bud cortex, whereas the septin ring was localized in the bud neck (Figure 2F), as reported previously (Okada et al., 2013). In contrast, during ER stress, septin translocation coincided with the dispersal of active Cdc42 (Figure 2F), indicating that active Cdc42 did not accumulate at

CRMs. Using time-lapse microscopy, we found that during normal growth, active Cdc42 accumulated in the growing bud of small-budded cells (Figure S2A; Video S5). In contrast, in time-lapse imaging of a stressed cell with a similarly sized bud, fluorescent signals of active Cdc42 dispersed within ~30 min and the bud did not grow (Figure S2B; Video S6).

### ER Stress Disperses Cdc42 from the Site of Polarized Growth, Disconnecting Its Upstream Effectors

To investigate the mechanism of how ER stress leads to the inactivation of Cdc42 from the site of polarized growth, we examined an upstream component, Cdc24, the GEF for Cdc42 (Figure 2G) (Hereford and Hartwell, 1974). In normal growing cells, Cdc24-GFP localized to sites of polarized growth including the incipient bud site in G1, the bud cortex in S and G2, and the bud neck in M phase (Figure 2H), as previously reported (Bos et al., 2007). In contrast, during ER stress the majority (66%) of cells had Cdc24-GFP moved to CRMs (Figures 2I and 2J).

Bud1/Rsr1 interacts with and activates Cdc24 at sites of polarized growth. Thus, we examined the active (GTP-bound) form of Bud1 using a split-yellow fluorescent protein (YFP) protein complementation assay (PCA) *in vivo*. In this assay, the YFP protein is split into two fragments and each non-fluorescent fragment is attached to a protein of interest, a bait, or a prey protein. The interaction of these two proteins brings together two YFP fragments and restores YFP fluorescence. Under normal growth, we observed YFP signals generated from Bud1-Cdc24 interactions at the bud tip and bud neck (Figure S2C, white arrowheads), consistent with previous reports (Park et al., 1997, 2002). During ER stress, we did not detect significant YFP signal either at the bud tip or the bud neck (Figure S2D: yellow arrowheads for loss of or reduced YFP signals). Together, our results suggested that while some Cdc24 remained at the bud neck, the majority no longer interacted with Bud1.

Similarly, we examined the Bud1-activating components Bud5 (a GEF for Bud1) and Bud2 (a GTPase-activating protein, GAP, for Bud1) by split-YFP (Figures S2E–S2H) (Marston et al., 2001; Nelson et al., 2012). YFP generated from Bud1-Bud5 was localized at the bud tip (G1 and S) and the bud neck (G2/M and M) (Figure S2E). YFP generated from Bud1-Bud2 was also localized at the bud tip (G1 and S) and the bud neck (Figure S2G), consistent with previous report for localizations for Bud5 and Bud2 (Kang et al., 2001). In contrast, neither

(B) Quantification of Myo1-GFP in WT cells grown normally or under ER stress (1  $\mu$ g/ml Tm) showed that Myo1-GFP moved with Shs1-RFP upon ER stress induction. Standard errors (SE) and statistical significances were calculated as described in STAR Methods unless otherwise stated. \* indicates  $p < 0.001$ .

(C) Bni5-GFP cells were grown without or with Tm. CRMs were visualized by CW staining.

(D and E) Spa2-GFP cells were grown without or with Tm. CW staining highlights the CRMs.

(F) Cells co-expressing an active Cdc42 biosensor (Gic2-PBD-RFP) and Shs1-GFP were grown with or without 1  $\mu$ g/ml Tm. Top, locations of active Cdc42 are indicated by white arrows; Shs1-GFP is shown by blue arrows. Bottom, quantification of the average fluorescence intensities of active Cdc42 (by Gic2-PBD-RFP) at the bud tip in cells grown with or without 1  $\mu$ g/ml Tm. Mislocalized Gic2-RFP is indicated with yellow asterisks. Measurements of Gic2-RFP levels were made for cells in each frame of time-lapse experiments shown in Figures S2A and S2B. Related to Figures S2A and S2B. See also Videos S5 and S6.

(G) Schematics of the Cdc42-activating Bud1/Rsr1 GTPase module.

(H and I) Localizations of Cdc24-GFP in different stages of the WT cell cycle, grown either without (H) or with Tm (I). Cdc24 at the bud tip or bud neck is shown by white arrows; mislocalized Cdc24-GFP is indicated with yellow asterisks. CRMs were also visualized by staining with CW. Representative cells from each stage of the cell cycle are shown.

(J) Quantification of the Cdc24-GFP localizations shown in (H) and (I). The y axis represents the ratios between the surface areas of buds and mothers; higher values indicate larger buds. The percentages of cells with the indicated localizations are shown above each column. Individual data points, as well as mean and SE are plotted, and the p value comparing localization of Cdc24-GFP to CRMs in untreated and treated samples was calculated. \* $p < 0.0001$ .

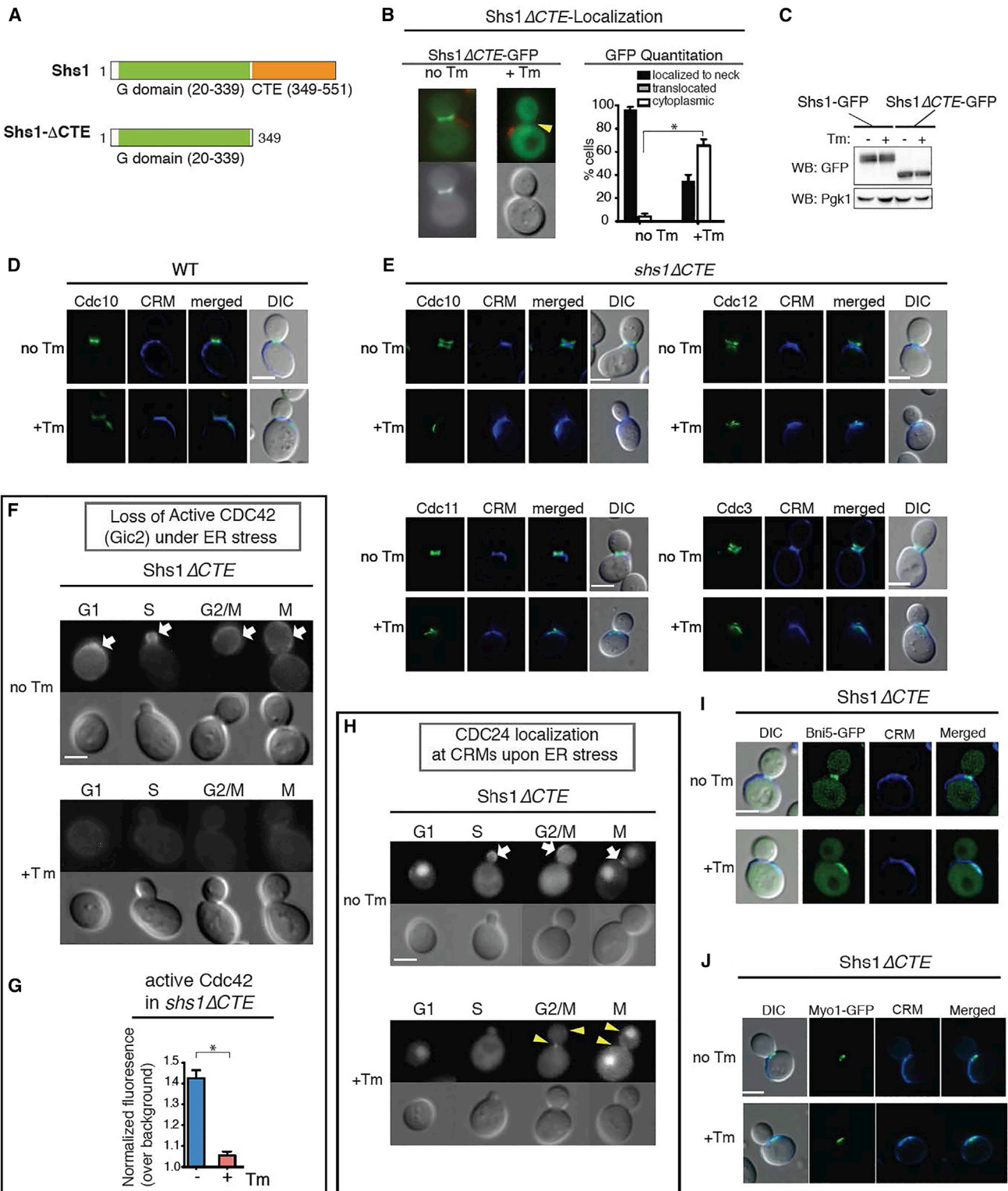


**Figure 3. The CTE of Shs1 Diminishes Shs1 to Move to Crms in Response to ER Stress**

(A) Domain organization of Shs1 (Versele and Thorer, 2004), the G domain, and GTPase binding. Shs1 $\Delta$ CTE lacks C-terminal end (CTE) of WT Shs1 (aa. 349–551).

(B) Shs1 $\Delta$ CTE-GFP is dispersed in cells grown with 1  $\mu$ g/ml Tm, while it is localized at the bud neck during normal growth. Arrowheads point absence of GFP localization. CW staining shows CRMs (red). Quantification of Shs1 $\Delta$ CTE-GFP in WT cells with or without 1  $\mu$ g/ml Tm. \* represents  $p < 0.0001$  comparing % of cells with dispersed Shs1 $\Delta$ CTE-GFP.

(legend continued on next page)

Bud1-Bud5 nor Bud1-Bud2 was localized at the site of polarized growth under ER stress (Figures 2H and S2F; yellow arrows indicated loss of interaction). Furthermore, we did not observe significant fluorescent signals at CRMs, indicating the absence of Bud1-Bud5 and Bud1-Bud2 interactions at CRMs. Taken together, these results showed that ER stress mislocalized Cdc24 to CRMs and attenuates the activity of the Bud1 GTPase.

### Not All Septin Subunits Are Required to Assemble at CRMs to Inactivate Cdc42

We next examined whether septin ring translocation to CRMs is critical for inactivation of either Cdc42 or its activating components. To this end, we generated a septin mutant that moved away from the bud neck but did not reach to CRMs during ER stress: a C-terminal truncation of the Shs1 septin subunit, Shs1 $\Delta$ CTE (CTE: C-terminal extension; Figure 3A). During normal growth, Shs1 $\Delta$ CTE-GFP was localized at the bud neck like WT Shs1-GFP (Figure 3B). However, upon ER stress induction ~70% of *shs1* $\Delta$ CTE cells had no detectable Shs1 $\Delta$ CTE localized at CRMs (Figure 3B). Shs1 $\Delta$ CTE-GFP expression levels were similar to WT Shs1-GFP even after ER stress induction (Figure 3C), revealing that Shs1 were dispersed throughout the cytosol. In contrast to Shs1, ER stress induction caused other septin subunits including Cdc3, Cdc10, Cdc11, and Cdc12 to move from the bud neck to the CRMs (Figure 3E). Taken together, these results revealed that the CTE of Shs1 is an important element for its translocation, but not other septin subunits, to CRMs in response to ER stress.

Do *shs1* $\Delta$ CTE cells support ER stress-induced block of polarized growth? In ER-stressed *shs1* $\Delta$ CTE cells, active Cdc42 was no longer present at the bud tip or the bud neck or any other locations including CRMs; (Figures 3F and 3G). Cdc24 in *shs1* $\Delta$ CTE cells, on the other hand, was mislocalized to CRMs at the extent similar to ER-stressed WT cells (Figure 3H). Thus, re-localizing the septin ring itself from the bud neck or molecular events associated with septin ring transfer from the bud neck contributes to the Cdc42 inactivation during ER stress. Furthermore, we tested the impact of ER stress on Bni5 in *shs1* $\Delta$ CTE cells (Figure 3I). We found that mislocalization of Bni5 also took place under ER stressed (Figure 3I). Similarly, Myo1 was also found at CRMs under ER stress (Figure 3J). Thus, the lack of Shs1 translocation to CRMs in *shs1* $\Delta$ CTE cells revealed that both polarized growth and cytokinesis was blocked under ER stress, at the extent similar to ER-stressed WT cells. Together, these data suggest that not all septin subunits are required to stop polarized growth and cytokinesis in response to ER stress.

### Translocation of Shs1 to CRMs Is Not Required to Induce the ERSU Pathway

Does the lack of Shs1 from CRMs affect the ERSU pathway in *shs1* $\Delta$ CTE cells? To answer this question, we assessed the extent of ER inheritance block upon ER stress induction (Figure S3A). We classified cells as previously published to three groups: small-budded cells (<2  $\mu$ m; Group I), medium-budded cells without nuclei (Group II), and large-budded cells with nuclei (Group III) (Babour et al., 2010; Piña et al., 2016; Piña and Niwa, 2015). As we found previously that ER stress has the most profound effect on Class I cells (Piña and Niwa, 2015), we focused on this class throughout this study. ER stress blocked ER inheritance in *shs1* $\Delta$ CTE cells at a level similar to that of WT cells (Figure S3A; lanes 1–2 for WT versus lanes 7–8 for *shs1* $\Delta$ CTE cells). Thus, the functional significance of the transfer of Shs1 along with all other septin subunits to CRMs itself or events associated with septin ring transfer to CRMs may reside beyond the initial stages of the ERSU pathway.

### Slit2 Is Required for ER Stress-Induced Cdc42 Inactivation in Both WT and Shs1 $\Delta$ CTE Cells

We reported previously that Slit2 is a component of the ERSU pathway and is important for cER inheritance block (Figure S3A) and septin ring translocation (Figure S3B) in ER stress (Babour et al., 2010; Piña et al., 2018). Here, we investigated the role of Slit2 in inhibiting polarized growth. In ER-stressed *slt2* $\Delta$  cells, Cdc42 (Figures S3C and S3D) and Cdc24 (Figures S3E–S3G) failed to move away from the site of polarized growth, demonstrating the requirement for Slit2 in blocking polarized growth. Cdc42 inactivation in *shs1* $\Delta$ CTE cells also depended on Slit2 (Figures S4A–S4C). In time-lapse experiments, Gic2-RFP remained localized at the bud tip (Video S7; Figure S4D, blue arrowheads; Figure S4E) even in ER-stressed *slt2* $\Delta$ *shs1* $\Delta$ CTE cells. A second bud emerged (red arrowheads) without cytokinesis of the first daughter cell. Furthermore, Cdc24 was localized to the second bud site regardless of ER stress (Figures S4F and S4G). Interestingly, we did not see any multi-budded *slt2* $\Delta$  cells; thus, truncation of CTE in *slt2* $\Delta$  cells caused a failure to block cytokinesis in the absence of SLT2. This is consistent with the ability of cell polarity components to affect the cytokinesis machinery (Wu et al., 2013). Interestingly, the septin ring visualized by Cdc11-GFP in ER-stressed *slt2* $\Delta$ *shs1* $\Delta$ CTE cells was fragmented (Figure S4B), rather than an intact form remaining at the initial bud site as observed in *slt2* $\Delta$  cells.

### Inactivating Cdc42 by SLT2 MAP Kinase Is Essential for Cell Survival under ER Stress

The above results revealed an unprecedented and essential role of the Slit2 MAP Kinase in the inactivation of Cdc42 during ER

(C) Western blot analysis of Shs1-GFP and Shs1 $\Delta$ CTE-GFP expression in cells with or without 1  $\mu$ g/ml Tm. Anti-Pgk1 was used as a loading control.

(D) CDC10-GFP in cells grown without or with Tm. All scale bars, 2  $\mu$ m.

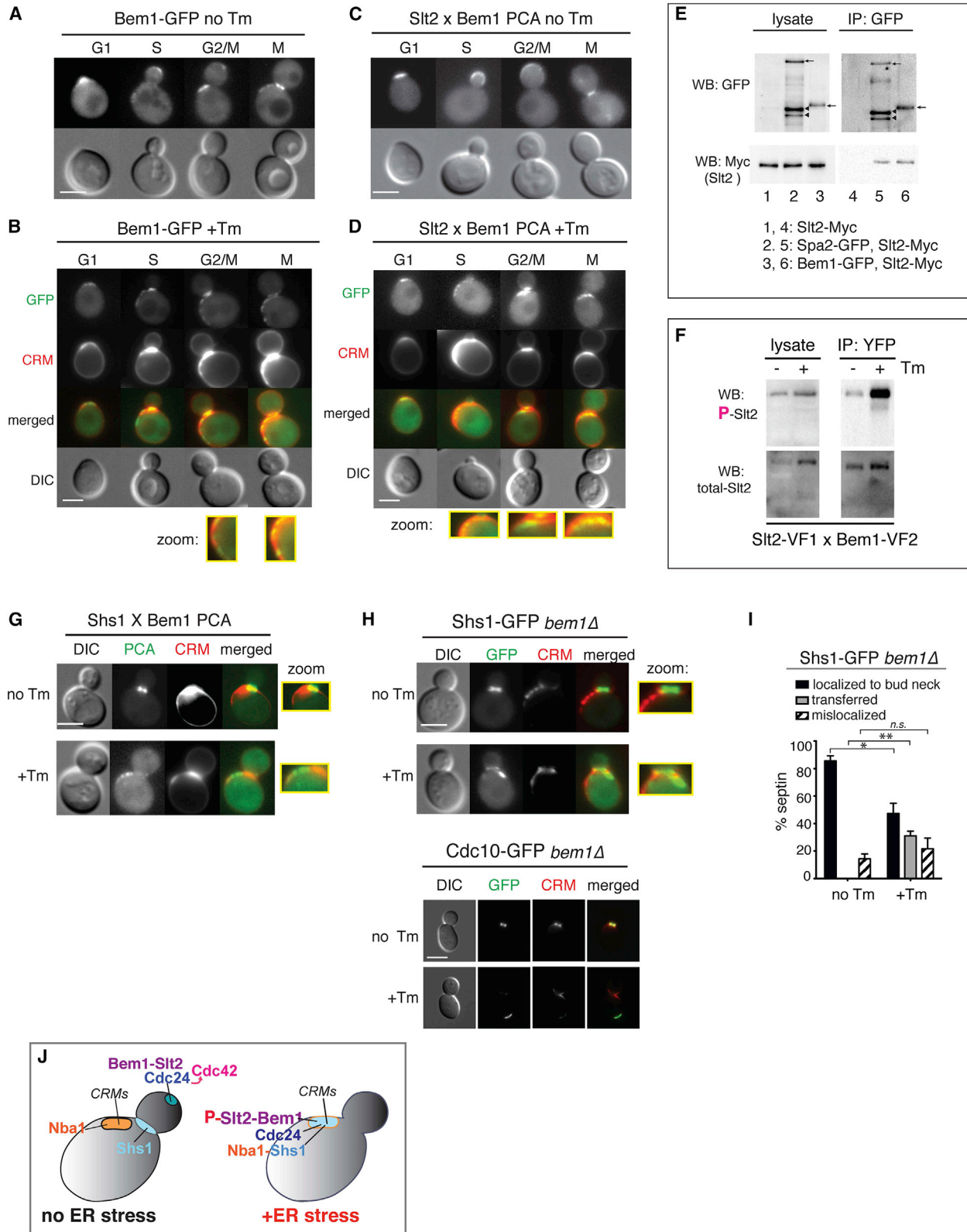
(E) *shs1* $\Delta$ CTE cells expressing GFP tagged septin subunits at their genomic loci. Cells were grown without or with Tm, with CRMs visualized by CW staining.

(F) Localization of Cdc42 (Gic2) in *shs1* $\Delta$ CTE cells that were either untreated (no Tm) or treated with 1  $\mu$ g/ml Tm. White arrows show the polarized localization of Gic2-GFP in unstressed cells, which was lost in ER-stressed cells.

(G) Quantification of active Cdc42-GFP fluorescence levels in *shs1* $\Delta$ CTE cells grown with or without 1  $\mu$ g/ml Tm. Mean and SE were calculated based on values from at least three independent experiments. \* represents  $p < 0.0001$  comparing normalized Gic2-GFP levels between unstressed and ER-stressed cells.

(H) Localization of Cdc24-GFP in *shs1* $\Delta$ CTE cells that were either untreated or treated with 1  $\mu$ g/ml Tm. ER stress caused mislocalization of Cdc24-GFP (yellow arrowheads).

(I and J) Bni5-GFP (I) and Myo1-GFP (J) in *shs1* $\Delta$ CTE cells were grown without or with Tm. CRMs were visualized by CW staining.



(legend on next page)

stress. To further evaluate the functional significance of this role, we tested whether inactivating Cdc42 via its inhibitor ML141 could rescue the growth of *slt2Δ* cells. Indeed, ML141 rescued the growth of both *slt2Δ* and *slt2Δ shs1ΔCTE* cells under ER stress (Figure S4H; compare +Tm versus +Tm+ML141). Significantly, ML141 treatment also rescued the ER inheritance block (Figures S5A and S5B, compare lanes 4 and 6) and septin transfer to CRMs (Figures S5C and S5D, compare lanes 4 and 6) in ER-stressed *slt2Δ* cells. These results are consistent with the idea that Slit2-induced Cdc42 inactivation is a hallmark of the ERSU pathway, coordinating with other ERSU events such as ER inheritance block and septin ring movement to CRMs to ultimately contribute to cell survival in response to ER stress.

### Split-DHFR Screen Identifies Slit2 Functional Partners in the ERSU Pathway

Under the normal growth, the importance of Slit2 is underscored by its involvement in a wide range of cellular functions, including genome silencing and cell wall responses (Chen and Thorner, 2007; Gustin et al., 1998). As a result, Slit2 is localized throughout the cell. This makes it challenging to delineate Slit2's specific role in the ERSU pathway. To this end, we performed a split-DHFR screen to quantitatively identify Slit2 binding partners *in vivo* (Tarasov et al., 2008). Split-DHFR is a growth-based selection assay, in which bait and prey proteins are each tagged with complimentary fragments of a mutated DHFR (mDHFR); if bait and prey proteins interact, the two fragments of mDHFR reconstitute into a fully functioning enzyme that is not inhibited by methotrexate, an inhibitor of the endogenous and essential yeast DHFR (Tarasov et al., 2008). Therefore, growth levels on methotrexate are proportional to the amount of reconstituted mDHFR enzyme and enable quantification of protein-protein interactions. Using this assay, we screened ~6,000 genes (Table S1) and identified 100 that showed enhanced interactions with Slit2 specifically during ER stress (Table S2).

### Bem1 Is a Unique Binding Partner for Slit2 during ER Stress

We further conducted gene ontology (GO) analysis on the top 100 interactors and categorized them according to their GO molecular functions (Figure S6A; Table S3) (Robinson et al., 2002).

We noticed that Bem1, Bnr1, and Vrp1 were the most connected genes (Figure S6A). Bem1 is an important polarity factor that functions as a scaffolding protein for Cdc24 and Cdc42, and recruits them to sites of polarized growth at both the bud tip and bud neck (Pruyne and Bretscher, 2000; Pruyn et al., 2004). Additionally, Bem1 is sequestered in CRMs by Nba1, which prevents it from binding to Cdc24, as a way of inhibiting Cdc42 recruitment to CRMs and of reducing the functional pool of Bem1 in cells (Meitinger et al., 2014). Thus, we focused on Bem1. Depending on which Bem1 pool Slit2 interacts with, we may be able to predict the functional significance of the Slit2-Bem1 interaction.

Using GFP-tagged Bem1, we found that Bem1 was localized at the bud tip in G1-S, and at the bud neck and CRMs in G2-M under normal growth (Figure 4A), in agreement with previous reports (Liu and Novick, 2014; Madden and Snyder, 1998; Smith et al., 2013; Toenjes et al., 2004). Upon ER stress induction, we observed Bem1-GFP primarily at the bud neck and CRMs, and only a small amount of Bem1-GFP remained at the site of polarized growth (Figure 4B). The loss of Bem1 localization at the bud tip is consistent with loss of activated Cdc42 (Gic2) from the bud tip and loss of polarized growth during ER stress (Figures 2F–2J).

These findings suggested that during ER stress, Slit2 might be recruited to CRMs by Bem1. We used split-YFP PCA in living cells to investigate. During normal growth, Slit2 interacted with Bem1 at sites of polarized growth, namely at the bud tip in small budded cells indicative of S phase, and the bud neck in large budded cells indicative of G2/M phases (Figure 4C). We further verified the interaction between Slit2 and Bem1 biochemically by co-immunoprecipitation (coIP). The amount of Slit2 co-purified with Bem1 was similar to that with Spa2, a protein known to interact with Slit2 (Figure 4E, compare lanes 5 and 6) (van Drogen and Peter, 2002). During ER stress, Slit2-Bem1 PCA was localized at CRMs (Figure 4D), suggesting that Slit2 interacted with the pool of Bem1 at CRMs.

It is known that Slit2 becomes phosphorylated and activated under ER stress (Babour et al., 2010). Given the dynamic localization of Slit2, we tested the activation status of Slit2 which was localized to CRMs under ER stress. We pulled down the Slit2-Bem1 interacting pair by their reconstituted YFP, and probed

### Figure 4. Bem1 Interaction with Slit2 Facilitates Translocation of Septin Rings at CRMs during ER Stress

- (A) Bem1-GFP in unstressed WT cells was localized to the bud tip, bud neck, and CRMs. All scale bars, 2  $\mu$ m.
- (B) Bem1-GFP localization was altered in Tm-treated WT cells. CRMs were visualized by staining with WGA-594. Zoomed-in views of Bem1-GFP at CRMs are shown.
- (C) Split-YFP PCA between Slit2 and Bem1 in untreated WT cells (no Tm).
- (D) Split-YFP PCA between Slit2 and Bem1 in cells treated with 1  $\mu$ g/ml Tm. Close-up views of Slit2 interacting with Bem1 at CRMs are also shown.
- (E) CoIP of experiment with Bem1-GFP and Slit2-Myc (lane 6). Spa2 is a previously identified Slit2 binding protein (lane 5).
- (F) The reconstituted YFP of the Slit2-Bem1 interaction (strain shown in [C] and [D]) was pulled down using anti-GFP beads. Cells were treated or untreated with Tm. Western blots for phosphorylated Slit2 (P-Slit2) and total Slit2 are shown.
- (G) Split-YFP PCA between Shs1 and Bem1 in untreated (no Tm) and Tm-treated WT cells. Close-up views show Shs1 interacting with Bem1 localized at the bud neck in untreated cells and at CRMs in Tm-treated cells. Zoomed-in views showing PCA signals at the bud neck for unstressed and at CRMs for ER-stressed cells are shown.
- (H) Shs1-GFP or Cdc10-GFP in unstressed cells was localized to the bud neck of *bem1Δ* cells, whereas Shs1-GFP or Cdc10-GFP was mislocalized away from the bud neck but was localized outside of CRMs in Tm-treated *bem1Δ* cells. Zoomed-in views show Shs1-GFP at the bud neck in unstressed cells and at a location distinct from CRMs in ER-stressed cells.
- (I) Quantification of Shs1-GFP in *bem1Δ* cells shows that significant levels of Shs1-GFP become mislocalized upon ER stress induction. \* $p < 0.01$ ; \*\* $p < 0.001$ ; ns, not significant.
- (J) Cartoon diagram summarizing the findings in this figure. Under normal conditions, Slit2 interacts with Bem1 at the bud tip while Shs1 is at the bud neck. None of these polarity components is seen at CRMs. When ER stress is triggered, Bem1 recruits Shs1 and phosphorylated Slit2 to CRMs.

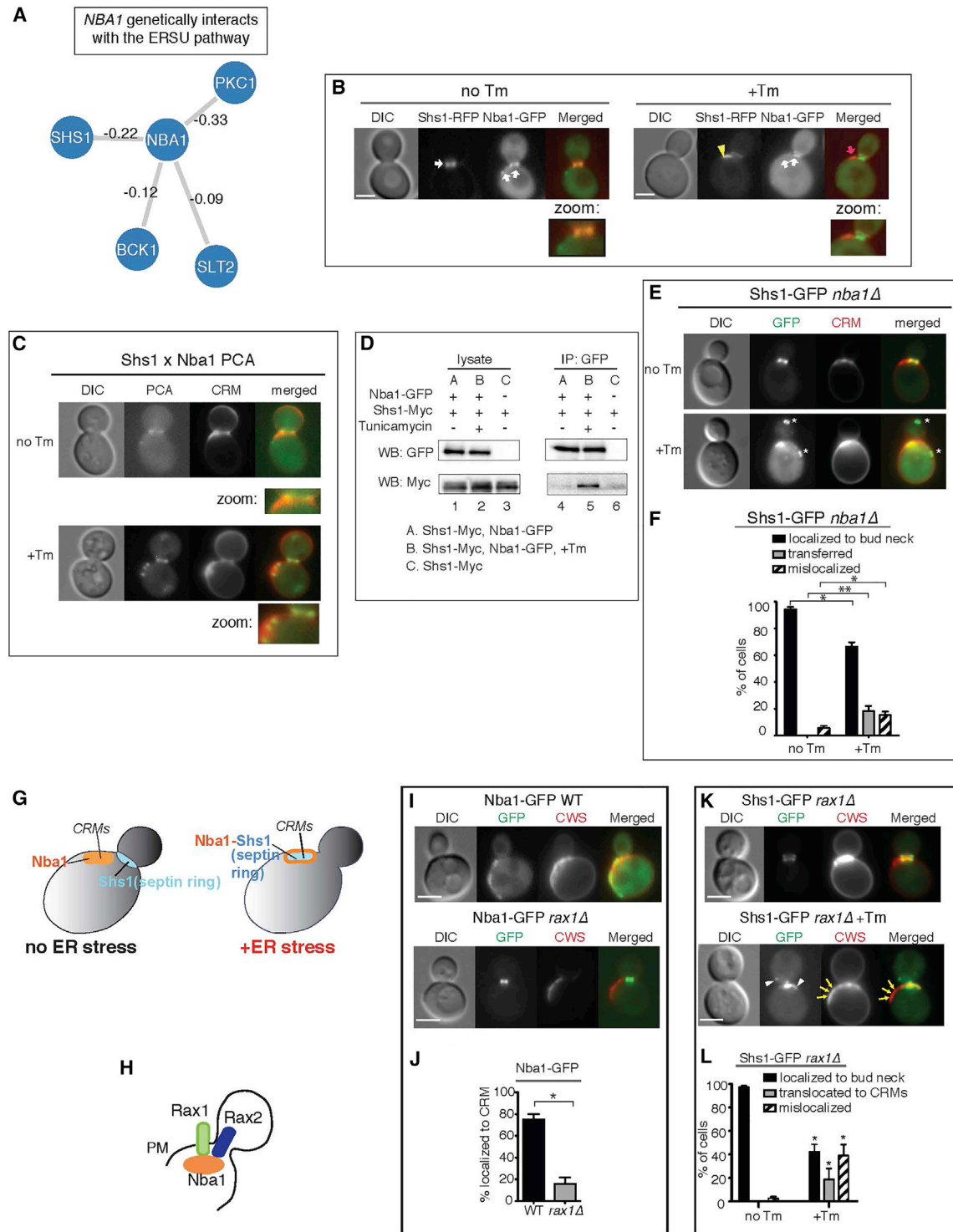


**Figure 5. Nba1 Recruits the Septin Ring to CRMs in ER Stress**

(A) Genetic interactions between *NBA1* and genes in the *SLT2* pathway as well as *SHS1* as identified by Costanzo et al., 2011. The strength of interactions are annotated on the lines.

(B) Nba1-RFP co-localizes with Shs1-GFP at the bud neck in untreated cells and at CRMs in Tm-treated cells.

(C) Split-YFP PCA between Shs1 and Nba1 in untreated (no Tm) and Tm-treated WT cells. Zoomed-in views show PCA signals at the bud neck in unstressed cells (no Tm) and at CRMs in ER-stressed cells (+Tm).

(D) We detected coIP of Shs1-Myc and Nba1-GFP only after Tm treatment of WT cells (lane 5). In untreated cells, little physical interaction between Shs1-Myc and Nba1 was detected (lane 4).

(legend continued on next page)

for phosphorylated Slit2 (P-Slt2). Interestingly, we found that the Bem1 bound P-Slt2 increased in ER stress (Figure 4F), suggesting that binding to Bem1 could provide a mechanism for activating Slit2.

### Bem1 Recruits the Shs1 Septin Ring Subunit to CRMs during ER Stress

Next, we tested if Shs1 interacted with Bem1 at CRMs during ER stress using the Split-YFP PCA. In unstressed cells, we observed fluorescent signals at the bud neck, revealing that Shs1 interacted with Bem1 at this location; however, during ER stress the fluorescence signals representing the Shs1-Bem1 interaction were located at CRMs (Figure 4G). Shs1-GFP and Cdc10-GFP failed to accumulate on CRMs in ER-stressed *bem1Δ* cells (Figure 4H), but rather mislocalized at a location outside of CRMs (Figure 4I), revealing the importance of Bem1 for the full septin ring transfer to CRMs.

### A Negative Polarity Regulator, Nba1, Remains at CRMs and Is Required for Shs1 Localization to CRMs under ER Stress

Our finding that Bem1 at CRMs binds to Slit2 and Shs1 was rather unexpected because Bem1 binding to Cdc24 at CRMs is normally prevented by Nba1, a recently identified CRM landmark (Meitinger et al., 2014). A genome-wide study revealed genetic interactions between Nba1 and Shs1 as well as components of the ERSU pathway, including Slit2, Bck1, and Pkc1 (Figure 5A) (Costanzo et al., 2011). This suggests that Nba1 is no longer found at CRMs in ER-stressed cells or that Nba1 undergoes ER stress induced changes to become an integral part of the ERSU pathway (Figure 4J).

Given our finding that Slit2, Shs1, and Cdc24 all found at CRMs under ER stress, we next tested if Nba1's localization would also change. We found that Nba1-GFP was localized to the bud neck and CRMs as reported (Meitinger et al., 2014), and that its localization did not change during ER stress (Figure 5B), consistent with Nba1's role as a landmark for CRMs. Using the split-YFP assay, we found that Shs1 and Nba1 interacted at CRMs only under ER stress (Figure 5C; +Tm). We also detected Shs1-Nba1 interaction using coIP, but the interaction was only significant in the presence of Tm (Figure 5D, compare lanes 4 and 5). Importantly, in *nba1Δ* cells, only 23% of cells showed a transferred septin ring in CRMs (Figures 5E and 5F), in contrast to ~50% in ER-stressed WT cells (Figures 1C and 1D). Thus, these results revealed a role for Nba1 in recruiting Shs1 to CRMs during ER stress (Figure 5G).

Two transmembrane proteins, Rax1 and Rax2, were reported to help localize Nba1 at CRMs (Figure 5H) (Meitinger et al., 2014). We confirmed that Nba1 localization at CRMs indeed depended on Rax1, but its localization to the bud neck did not (Figures 5I and 5J). If bud neck-localized Nba1 is sufficient to target the translocated septin ring to CRMs during ER stress, we would not expect *RAX1* deletion to affect septin translocation. To differentiate which populations of Nba1 are responsible for mediating septin ring translocation during ER stress, we tested Shs1-GFP localization in ER-stressed *rax1Δ* cells. We found that Shs1-GFP remained at the bud neck, or mislocalized outside of CRMs in ER-stressed *rax1Δ* cells (Figures 5K and 5L), indicating that Nba1 in CRMs is critical for septin ring translocation to CRMs.

### The functional Significance of the Complete Septin Ring Localization at CRMs

Our results so far revealed that polarity components undergo significant changes under ER stress. We next investigated the functional significance of the septin ring transfer to CRMs by comparing WT and *shs1ΔCTE* cells. ER inheritance block occurred normally in response to ER stress in both WT and *shs1ΔCTE* cells (Figure S3A). Thus, we tested a later event: the ability of cells to re-enter the cell cycle after ER functional homeostasis is re-established. In order to test whether *shs1ΔCTE* cells are able to re-enter the cell cycle in a manner similar to WT cells after recovery from ER stress, we devised an ER stress-recovery assay (Figure 6A). In this method, we first treated cells with Tm for 2 hrs, then washed Tm away before starting the recovery time course. At 4 min after washing out Tm and starting ER stress recovery, the septin ring re-appeared at a new location (Figures 6B and 6C, white arrow). This was followed by the emergence of a new bud after ~50 min of recovery time (Figure 6C, blue arrow, Video S8). This result is in agreement with our previous report that the original daughter cell is never re-used when cells recover from stress (Babour et al., 2010). As the original daughter cell was not utilized, we observed two budded cells upon recovery, but the septin ring was only localized to the bud neck of the newly emerged daughter cell (Figure 6D).

Furthermore, during recovery, activated Cdc42 was polarized to the new presumptive bud site (Figure 6E; Video S9). These results are consistent with our observation that the previously translocated septin ring moved from CRMs to a new incipient bud site, allowing cells to re-enter the cell cycle. As such, we most frequently observed new daughters emerged from sites adjacent to CRMs in these recovery assays.

In contrast to WT cells, both the re-appearance of the septin ring and bud emergence in *Shs1ΔCTE* cells were significantly

(E) Nba1 is required for Shs1-GFP localization at CRMs during ER stress. Shs1-GFP in untreated (no Tm) or Tm-treated (+Tm) *nba1Δ* cells is shown.

(F) Quantification of Shs1-GFP in unstressed and ER-stressed *nba1Δ* cells. \**p* < 0.05; \*\**p* < 0.005.

(G) Cartoon diagram summarizing the results. Nba1 recruits Shs1 to CRMs during ER stress.

(H) Rax1 and Rax2 are important for localization of Nba1 to the CRMs at the plasma membrane (PM) (Meitinger et al., 2014).

(I) Nba1-GFP localization in WT or *rax1Δ* cells. The loss of *RAX1* (*rax1Δ*) significantly diminished Nba1-GFP localization to CRMs and Nba1-GFP remained at the bud neck.

(J) Quantitation of Nba1-GFP localized at CRMs. t test showed that Nba1-GFP localizations to CRMs was significantly reduced in *rax1Δ* compared to WT (\* represents *p* < 0.0015).

(K) Shs1-GFP localization in untreated and Tm-treated *rax1Δ* cells. Shs1-GFP localizes to the bud neck during normal growth and remained at the bud neck in ER-stressed *rax1Δ* cells.

(L) Quantification of Shs1-GFP localization in (K). *p* values from t tests comparing each of the Shs1-GFP localizations between no Tm and +Tm conditions is shown (\* represents *p* < 0.001).

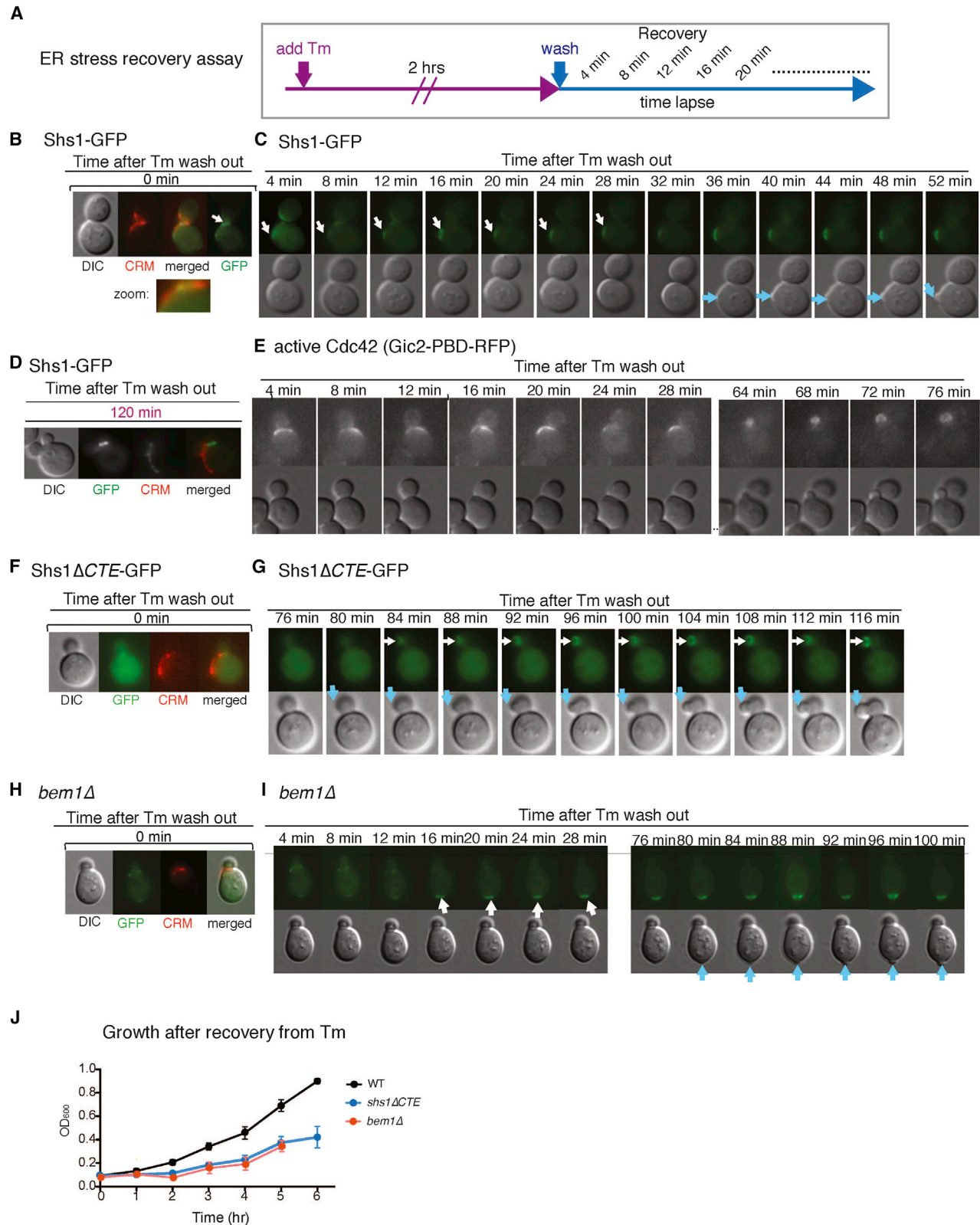


**Figure 6. The CTE of Shs1 Dictates Re-entry to the Cell Cycle When ER Stress Is Recovered**

(A) Experimental design for the ER stress recovery assay. Cells expressing Shs1-GFP were treated with 1  $\mu$ g/ml Tm for 2 h. Then, Tm was removed by washing the cells with SC medium. Next, cells were monitored by live-cell imaging. In this assay, CRMs were visualized by staining with WGA-594.

(legend continued on next page)

delayed after recovery from ER stress (Figures 6F and 6G; Video S10). The slower kinetics of the re-appearance of the septin ring after Tm removal and the new bud emergence was further reflected in the slower growth during the recovery phase of 6 hrs (Figure 6J). Another striking difference with *shs1 $\Delta$ CTE* cells was the specific location of the bud emergence: the new daughter cell emerged from within the existing daughter cell, instead of emerging from the mother cell as in WT (Figures 6C and 6G).

We further tested the importance of septin ring movement to CRMs in *bem1 $\Delta$*  cells, in which Shs1-GFP moved to a discrete location outside of CRMs under ER stress (Figures 4H and 6H; Video S11). Interestingly, during the recovery process, Shs1-GFP did not depart from the transferred location. Instead, the new bud emerged at this same location, although the kinetics of the bud emergence was significantly delayed at the extent similar to *shs1 $\Delta$ CTE* cells (Figures 6H and 6I). Thus, these results unveiled that the transfer of the septin ring from the bud neck specifically to CRMs is important for timely recovery and re-entry into the cell cycle.

### The Impact of Aging on ERSU Cells

Establishment of a negative polarity cue (or disruption of a polarity cue) by ER stress-induced septin ring subunit translocation to CRMs raises an intriguing question regarding aged cells with multiple CRMs. After each cell division, CRMs accumulate on the cortex of the cell. Thus, aged cells have accumulated multiple CRMs (Powell et al., 2003; Sinclair et al., 1998). Taking this into account, how might aged cells respond to ER stress-induced septin ring translocation? Among asynchronously growing cells, over 50% are naive cells with only the birth scar (we refer to these as “young cells”). Here, we examined how ER stress impacts cells that have more than three CRMs (we refer to these as “aged cells”). First, we quantified the levels of Nba1 at each bud scar in aged cells (Figures 7A and 7B). Although Nba1-GFP was present at each bud scar, it was highest in the one most proximal to the bud neck (Figure 7B), consistent with a previous report (Meitinger et al., 2014). Based on our finding that Nba1 is a binding partner of Shs1 at CRMs, we tested if the septin ring might transfer to the most recent CRMs during ER stress. In aged cells grown in regular growth medium, the septin ring remained localized at the bud neck (Figure 7C). Upon ER stress induction, the septin ring transferred frequently (~60%) to the proximal bud scar, and less frequently (~20%)

to distal ones (Figures 7C–7E), indicating that septin ring transfer tends to occur in correlation with higher Nba1 levels.

### Age Impacts the Ability to Undergo ER Stress Recovery

We next examined the consequence of translocating the septin ring to distal bud scars. Using the recovery assay (Figure 6A), we monitored ER-stressed and aged cells with septin ring translocated to the distal bud scar (Figures 7F and 7G). Upon removal of the ER stress-inducing drug, the translocated septin ring moved away from the distal bud scar and re-localized to the more recent (proximal) bud scar (Figures 7F and 7I; Video S12). Ultimately, septin rings ended up at the most proximal site to the bud neck through stepwise re-localization of bud scars in the middle. The amount of time required for aged cells to translocate the septin ring from the distal CRM to the most recent (proximal) CRM was significantly delayed when compared to naive cells (Figure 7I). Strikingly, despite the translocation of septin rings, we did not observe the emergence of a new daughter cell even after 120 min of ER stress recovery (Figure 7G). This is in stark contrast to naive WT cells, where we detected re-entry into the cell cycle, scored by new bud emergence, within 90 min. Importantly, the recovery kinetics for aged WT cells was even slower than for *shs1 $\Delta$ CTE* cells (Figure 6G). Thus, while ER stress-induced re-localization of septin ring could occur, the presence of multiple bud scars in aged cells diminished the ability of the cells to re-enter the cell cycle.

## DISCUSSION

One of the most important elements of cell survival is the correct segregation of cellular contents during cell division. Previously, we reported that the ERSU pathway, a cell-cycle checkpoint, ensures the inheritance of functional ER during the cell cycle (Babour et al., 2010; Piña et al., 2016, 2018; Piña and Niwa, 2015). When the ER is stressed, the ERSU pathway blocks the inheritance of stressed ER and cytokinesis, thereby preventing the generation of cells lacking sufficient levels of functional ER. Our previous work uncovered that the cytokinesis block occurs by mislocalization of the septin ring, a critical component of cytokinesis; however, the mechanism of this mislocalization and its potential role beyond cytokinesis block remained elusive. Here, we found that this movement of septin rings to CRMs occurs by partially overriding the Nba1-dependent negative polarity establishment component. In addition, we found that Nba1

(B and C) Recovery assay for WT cells expressing Shs1-GFP according to (A) to follow septin dynamics (Shs1-GFP) and bud emergence. The first frame of the time-lapse (time 0) is shown in (B) along with CRM staining. Subsequent frames are shown in (C). White arrow indicates Shs1-GFP. Blue arrow indicates newly emerging bud. Related to Video S8.

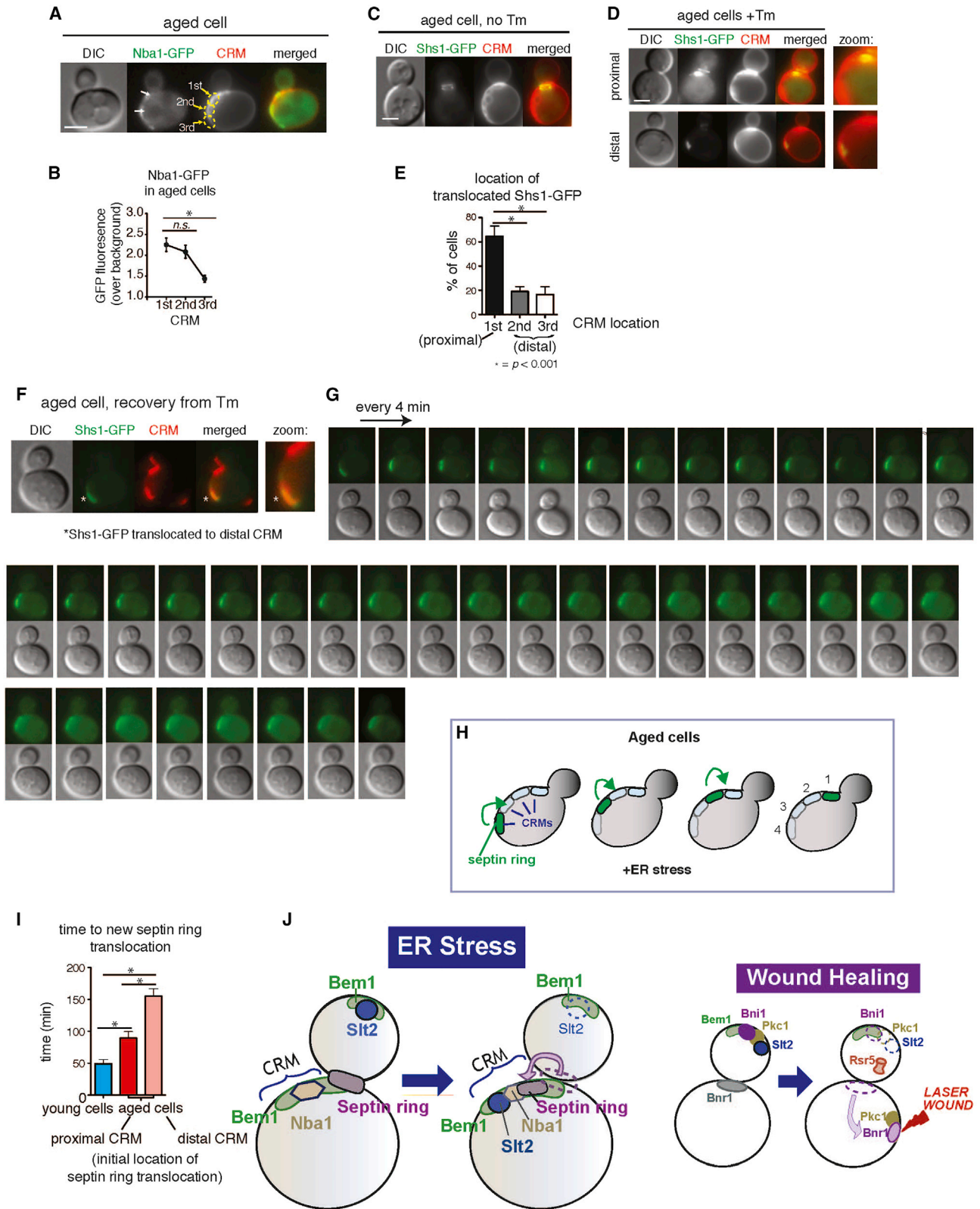
(D) Location of Shs1-GFP and CRMs in WT cells upon ER stress recovery for 120 min. As cells re-enter the cell cycle, a new bud emerges and Shs1-GFP localizes to the new bud. The initial bud was not re-used even after cells recovered from ER stress.

(E) Recovery assay to monitor active Cdc42 (Gic2-PDB-RFP) in WT cells according to (A). Active Cdc42 started to appear within 4 min after Tm wash. Active Cdc42 appeared at the newly emerging bud cortex at ~64 min after Tm wash. Related to Video S9.

(F and G) Recovery assay for Shs1- $\Delta$ CTE-GFP, which remained dispersed immediately after Tm recovery. The first frame of the time-lapse (time 0) is shown in (F) along with CRM staining. Subsequent frames are shown in (G). White arrow indicates Shs1-GFP and blue arrow shows a new bud. Related to Video S10.

(H and I) Dynamics of ER stress recovery of *bem1 $\Delta$*  cells. ER stress recovery assay for *bem1 $\Delta$*  cells was done according to Figure 6A. The first frame of the time-lapse (time 0) is shown in (H) along with CRM staining. Subsequent frames are shown in (I). White arrow indicates Shs1-GFP. Blue arrow indicates bud emergence after recovery. Related to Video S11.

(J) Growth of WT, *shs1- $\Delta$ CTE*, or *bem1 $\Delta$*  cells after ER stress recovery. Mean and SE were calculated based on values from at least three independent experiments.



(legend on next page)

allows Bem1 at CRMs to bind Cdc24 and Slt2; thus, CRMs serve as sites to gather key components in anticipation of cell-cycle re-entry. Under normal growth, Nba1 at CRMs blocks both septin ring formation and Cdc24 association to CRM-localized Bem1, leading to the block of Cdc42 activation for polarized growth (Meitinger et al., 2014). Under ER stress, Nba1 is required for septin ring transfer to CRMs. Furthermore, Nba1 allows Cdc24 to associate with Bem1, while still preventing Cdc42 from being activated at CRMs. Bem1 localized at CRMs serves as the only binding site for activated Slt2, an ERSU MAP kinase. Taken together, our findings suggest that previous cell division sites, CRMs, serve as reservoir or an “ER stress recovery preparation” site, for gathering components that aid in “cell-cycle re-entry” upon ER stress recovery.

Our study here demonstrated that the septin ring transfer to CRMs in response to ER stress is important for the timely re-entry into the cell cycle. Furthermore, the ring must contain all five septin subunits. During the initial translocation steps upon ER stress induction, *shs1ΔCTE* cells could retain a partial septin complex at CRMs and missing only one subunit, Shs1 (Figure 3E). It is possible that the CTE of Cdc11 could replace the function of Shs1-CTE here (Finnigan et al., 2015). Nonetheless, *shs1ΔCTE* cells are much delayed in the cell-cycle re-entry, when compared to WT cells, suggesting that Cdc11-CTE could not completely cover for the loss of Shs1-CTE. The molecular basis of how the presence of the intact septin ring at CRMs ensures timely re-entry into the cell cycle will require further investigation. In this regard, recent studies have shown that septins are involved in other aspects of cell polarity, including (1) the formation of cytoskeletal scaffolding structures (Mostowy and Cossart, 2012); (2) the formation of a diffusion barrier in the plasma membrane and ER (Caudron and Barral, 2009); and (3) lending definition to daughter-cell differentiation during bud emergence (Okada et al., 2013), in addition to the well-known role of septin rings in polarized growth and cell division (Hartwell, 1974). All of these functions require septin rings to act as relatively static and passive landmarks during most of the cell cycle. The lack of septin ring formation at the bud neck prior to budding should trigger the Swe1-dependent morphogenesis checkpoint or mitotic delay (Barral et al., 1999). This highlights the importance of the timely placement and generation of the septin ring

at the site of polarized growth for initiating a new round of the cell cycle. By contrast, an unprecedented translocation of septin rings to CRMs enables cells to retain cellular abilities to re-enter cell cycle during the ER stress.

Based on time-lapse experiments, septin ring translocation to CRMs appears to occur via a transfer of a septin ring complex that is initially formed at the bud neck. In response to ER stress, we noticed that the diameter of the septin ring complex appeared to become smaller than the septin ring at the bud neck prior to ER stress. This suggests that ER stress causes a septin ring to take a more compact structure, allowing for increased mobility. Alternatively, some of the septin subunits may disassemble from the bud neck to generate a different septin ring at CRMs. At this point, we cannot rule out the possibility that some of the septin subunits disassemble at the bud neck and reassemble to a ring at CRMs. Supporting such a mechanism, a previous study showed that septin ring subunits gradually transfer from the previous bud neck to the incipient bud site (Chen et al., 2011). Regardless of the mechanism, an important factor that distinguishes ER stress-induced septin ring is its transfer to CRMs rather than to the incipient bud site.

The translocation of septin rings at CRMs also accompanied other unexpected changes. Under normal growth, septin ring formation is coordinated with polarized cell growth. Under ER stress, the presence of septin rings at CRMs was not associated with bud emergence or polarized bud growth. Furthermore, under normal growth conditions, yeast cells have an elaborate mechanism involving a Cdc42 antagonist, Nba1, that prevents polarized growth from CRMs by interfering with the Cdc24 association with Bem1 localized at CRMs. Surprisingly, we found that Nba1 remained localized at CRMs under ER stress, but might have undergone certain character changes while retaining other features. For example, septin ring formation is normally coordinated with Cdc42 activation and polarized bud growth, but these events did not take place in septin rings transferred at CRMs under ER stress. Further, both Cdc24 and Slt2, but not Cdc42, localize to CRMs upon binding to Bem1. These results reveal that ER stress incapacitates a part of Nba1 functions, such that septin ring formation and Cdc24 localization can take place while Cdc42 activation or initiating polarized growth are continued to be blocked.

### Figure 7. Septin Ring Behaviors in Aged ER-Stressed Yeast Cells with Multiple Bud Scars

(A and B) Nba1-GFP localization in Tm-treated (1  $\mu\text{g}/\text{ml}$ ) “aged” cells (A) and quantification of Nba1-GFP signals at different CRMs (B). Note that “aged cells” refers to cells two or more CRMs. “1st,” “2nd,” and “3rd” refer to the position of the CRM relative to the bud neck. p values comparing differences in GFP levels are indicated as: ns, not significant; \*,  $p < 0.001$ .

(C–E) Shs1-GFP localization in aged cells that were (C) untreated or (D) treated with Tm. Quantification of Shs1-GFP localization at each CRM is shown in (E). “Proximal” and “distal” refers to the location of the CRM relative to the bud neck. p values comparing differences in % of cells are indicated as \*,  $p < 0.001$ .

(F and G) ER stress recovery assay for “aged cells” with Shs1-GFP transferred at the distal location. The first frame of the time-lapse (time 0) is shown in (F) along with CRM staining. Subsequent frames are shown in (G).

(H) Graphical representation of septin ring transferred to the distal CRM during the time lapse experiment shown in (F) and (G).

(I) Average time required for the reappearance of the septin ring at the new bud site, which was indicative of re-entry into the cell cycle, after ER stress recovery. p values were calculated to compare young cells and aged cells, and to compare aged cells with septin ring at either proximal or distal CRM prior to recovery in % of cells. \*,  $p < 0.001$ .

(J) In order for cells to effectively survive “ER stress,” a cellular strategy of hijacking the components that support cell growth and temporarily re-assembling them at a different location as an emergency complex allows proper handling of ER stress. Specifically, mobilizing components involved in the polarized growth at the bud tip, such as Bem1, Cdc24, and Slt2, and their re-assembly at CRMs along with association with the septin ring will achieve cell-cycle halting while re-establishment of the ER functions is handled. Mobilization and re-formation of the polarized cell growth components may be a general emergency strategy for cells to cope with different types of stress or catastrophe. In response to a laser-induced wound, for example, components involved in polarized growth, such as Bni1 and Pkc1 (an upstream kinase of Slt2 MAP kinase), become mobilized from the bud tip, and their re-localization at the wound site allows for wound healing while cell growth is temporarily halted (Kono et al., 2012).

How can Bem1-Cdc24 be localized at CRMs in the presence of Nba1? Previous studies have shown that Bem1 serves two main scaffolding functions: (1) for the Cdc42 GEF, Cdc24; and (2) for Cdc42 effectors such as Cla4 or Ste20, which are p21-activated kinases (PAK) (Atkins et al., 2008; Kozubowski et al., 2008). PAK phosphorylates Cdc42 during polarized growth in yeast cells. This process helps ensure that the temporal and spatial regulation of Cdc42 activity determines the site and timing of symmetry breaking on the cell surface. Even after bud emergence, Bem1 remains at the bud tip until the direction of bud growth switches from an orthogonal to a bilateral direction. Our finding that Bem1 interacts with activated Slit2 during ER stress suggests that Slit2 may mediate one of the molecular switches that disassembles the Bem1-Cdc24 complex from the bud tip and assembles it at CRMs. Interestingly, Slit2 appears to be temporally activated during the cell cycle at around the time when the polarized growth switches directions even in the absence of ER stress (Li et al., 2010). Thus, under normal growth, the Slit2-Bem1 association may ultimately dictate Cdc42 activity in a spatially and temporally regulated manner to establish a switch for polarized growth. Upon ER stress activation, the Slit2-Bem1 interaction occurred at CRMs, which, as a consequence, may generate “hyper-activated” Bem1 or partially weaken Nba1 function. Thus, this process somehow facilitates Bem1-Cdc24 to localize to CRMs even in the presence of Nba1. The continued presence of Nba1 may contribute to disconnecting the activation of Cdc42. Furthermore, the interaction of Bem1, Cdc24, and activated Slit2 might allow septin ring subunits to translocate to CRMs even in the presence of a negative regulator such as Nba1. These observations are consistent with the idea that septin ring translocation to CRMs also requires Bem1.

Importantly, the lack of a “ER-stress recovery complex” at CRMs in ER-stressed *bem1Δ* or *shs1-ΔCTE* cells underscores the functional significance of concentrating Slit2, Cdc24, and all five septin subunits at CRMs under ER stress. In both cases, the absence of translocated Shs1 at CRMs significantly delayed the cell’s ability to re-enter the cell cycle even when ER function is re-established. Thus, ER stress-induced Shs1 transfer to CRMs represents a key event in anticipation of re-established cellular competence of resuming cell-cycle division following ER stress recovery. Interestingly, upon re-entry into the cell cycle, we found that the original daughter cell was never utilized. Instead, a new second bud emerged from the original mother cell. Under normal growth, establishing polarized growth requires an intrinsic competition between different foci of activated Cdc42 and its upstream GEFs and GAPs, which are aided by positive feedback to establish the “winning” foci for polarized growth that leads to the bud’s emergence from that foci (Wu et al., 2015). Once ER functional homeostasis is re-established, polarized growth can be re-established by re-mobilizing these components to the outside of the inhibitory zone that is defined by CRMs. Indeed, we found that upon recovery from ER stress new buds emerged from the sites directly adjacent to CRMs, retaining the usual axial budding pattern seen in haploid yeasts. The kinetics of the cell-cycle recovery was significantly diminished in both *shs1-ΔCTE* and *bem1Δ* cells, in which the complete septin ring, Bem1, Cdc24, and Slit2 failed to gather at CRMs upon ER stress. Thus, these findings underscore the functional significance of strategically

localizing key components at CRMs for resuming polarized growth in order to re-enter the cell cycle.

An interesting implication associated with CRMs as the site of septin ring translocation is aging, as cells accumulate CRMs as they undergo replication cycles. Therefore, unlike young cells, aging mother cells with multiple CRMs provide more choices for septin rings and other key components to congregate. Although young and aged cells appear to be equally effective at translocating septin rings, older cells with multiple CRMs struggle at re-localizing septin rings during recovery. Nba1 is present in several CRMs in such older cells. In addition, as cells age further, some of the CRMs may not have Nba1, which could alter the nature of septin ring transfer to occur at CRMs. One of the challenges of septin ring transfer to CRMs with decreased levels of Nba1 or little Nba1 includes strategies to block polarized growth. Interestingly, UPR activation is also significantly slower in older cells (data not shown). Whatever the mechanisms might be, the prolonged kinetics of ER stress and UPR induction may provide additional time to gather components key to cell-cycle re-entry. We found that septin rings transferred to older CRMs and then kept moving between CRMs until they reached the most recent CRMs before re-initiating the cell cycle. This might reveal that Nba1 concentration dictates the establishment toward recovery state. Furthermore, strong evidence suggests that during replicative aging, aging factors such as extra-chromosomal DNA circles and damaged-protein aggregates that decrease fitness of aged cells accumulate asymmetrically in the aging mothers (Erjavec et al., 2007; Higuchi-Sanabria et al., 2014; Shcheprova et al., 2008; Singh et al., 2017; Spokoini et al., 2012); this may also contribute to the delay of re-entry into the cell cycle during ER stress.

There is a precedent for a molecular strategy to respond to cellular emergencies by re-directing polarized cell growth components. For example, the mobilization or re-organization of Bni1—which regulates polarized cytoskeleton and Pkc1, an upstream kinase of Slit2—plays a major role in recovery from a laser-induced wound on the cell surface of yeast (Kono et al., 2012) (Figure 7J). The driving force behind halting polarized growth and mobilizing the necessary components for cell membrane surface repair is generated from rapidly degrading Bni1, a formin that nucleates actin filaments, via proteasomes. Concomitantly, Bnr1, another formin is mobilized to reach to the wound site to generate a “wound recovery complex” along with Pkc1. A conceptual parallel can be found in ER-stressed cells: in response to ER stress, re-localization of Bem1, Slit2 kinase, and Cdc24 from the bud tip to CRMs is coordinated with the timely induction of the ERSU pathway. Re-establishment of the polarized growth and a platform for inheritance of the ER in the emerging daughter cell can be facilitated by the presence of this “ER stress recovery complex” at a reservoir of regulators of polarized growth at CRMs. Thus, our ER stress studies and those examining laser-induced wounds may have revealed an underlying principle and cellular strategy of handling catastrophes: by linking cell growth with the handling of a specific cellular stress, cells mobilizing components involved in polarized cell growth and re-functions them to take care of a specific cellular stress. Such a strategy ensures a break on the continued growth and provides effective means to handle stress recovery. One important element of such a stress-handling strategy is to retain

the ability to resume polarized growth. CRMs may provide an ideal location for transferring ER stress recovery complex under ER stress in the absence of specific targets such as wounded sites in the cell.

Finally, as ER stress is conserved among eukaryotic cells, it is tempting to speculate that a similar mechanism might exist for effectively handling ER stress in mammalian cells. While the molecular basis of the CRM and its constituents are unique to yeast cells, recent studies have suggested that the mid body (MB) formed at the cleavage furrow during cytokinesis may be a functional equivalent of CRMs (Chen et al., 2013; Ettinger et al., 2011; Kuo et al., 2011; Pohl and Jentsch, 2009; Thieleke-Matos et al., 2017). Structurally, the MB takes a ring-like shape that resembles CRMs. As CRMs represent prior cytokinesis sites, the MB is also formed during cytokinesis and plays a role in cell division. While the exact MB constituents differ from those of CRMs, recent studies revealed that the MB also retains the post-mitotic structure. Specifically, upon division of mammalian two daughter cells, the MB ends up in one of the daughter cells. Ultimately, many MBs can be removed from the cell by a few mechanisms including autophagy, although its half-life appears to differ depending on the cell type. The half-life of an MB appears to dictate the pluripotency of stem cells. For example, stem cells with a long-lived or persistent MB normally retain pluripotency. By contrast, during asymmetric division of stem cells, in which one cell retains pluripotency and the other differentiates into a specific cell type, the extent of potency is correlated with the half-life of the MB. Given our findings on CRMs, it will be interesting to test if pluripotency of MBs change in response to ER stress.

## STAR★METHODS

Detailed methods are provided in the online version of this paper and include the following:

- KEY RESOURCES TABLE
- LEAD CONTACT AND MATERIALS AVAILABILITY
- EXPERIMENTAL MODEL AND SUBJECT DETAILS
- METHOD DETAILS
  - Plasmid Construction
  - Light Microscopy techniques
  - Electron Microscopy
  - Split-DHFR Screen
  - Co-purification Assays
  - Yeast Spot Assays
  - Quantification of Microscopy Images
  - Statistical Analysis
  - Gene-Set Enrichment Analysis for Split-DHFR Screen

## SUPPLEMENTAL INFORMATION

Supplemental Information can be found online at <https://doi.org/10.1016/j.devcel.2019.08.017>.

## ACKNOWLEDGMENTS

We thank Dr. Stephan Michnick for the DHFR libraries. The work was supported by grants from the NIH (R01GM087415), UCSD Chancellor Excellent Scholarship (formally FISP), and the UCSD Academic Senate fund to M.N.;

and by grants from Volkswagen Foundation “Life” grant and a The Deutsche Forschungsgemeinschaft (DFG) grant (SFB1190) to M.S. J.T.C. and F.P. were supported by a UCSD Molecular Biology Cancer postdoctoral fellowship and an NIH 5T32AI007469-20UCSD/LIAI allergy postdoctoral training grant, respectively. M.S. is an incumbent of the Dr. Gilbert Omenn and Martha Darling Professorial Chair In Molecular Genetics. We also thank Jon Mulholland and John Perrino (Stanford University Cell Sciences Imaging Facility) for assistance with electron microscopy.

## AUTHOR CONTRIBUTIONS

M.N. conceived the idea, analyzed the results, guided and organized the work, and wrote the manuscript. J.T.C. conceived the idea, performed the experiments, analyzed the data, and wrote the manuscript. M.S. proposed, analyzed the DHFR experiment, and provided advice on data interpretation. Y.C. performed the DHFR experiment and the data analyses. M.O. performed the EM experiments and provided general advice on the yeast septin, septum, and cytokinesis. F.P. performed a significant portion of the experiments, and Y.-S.L. performed additional experiments during the review process. Funding secured by M.N. All authors commented.

## DECLARATION OF INTERESTS

The authors declare no competing interests.

Received: November 17, 2018

Revised: May 19, 2019

Accepted: August 23, 2019

Published: September 26, 2019

## REFERENCES

- Atkins, B.D., Yoshida, S., and Pellman, D. (2008). Symmetry breaking: scaffold plays matchmaker for polarity signaling proteins. *Curr. Biol.* *18*, R1130–R1132.
- Babour, A., Bicknell, A.A., Tourtellotte, J., and Niwa, M. (2010). A surveillance pathway monitors the fitness of the endoplasmic reticulum to control its inheritance. *Cell* *142*, 256–269.
- Bähler, J., Wu, J.Q., Longtine, M.S., Shah, N.G., McKenzie, A., 3rd, Steever, A.B., Wach, A., Philippsen, P., and Pringle, J.R. (1998). Heterologous modules for efficient and versatile PCR-based gene targeting in *Schizosaccharomyces pombe*. *Yeast* *14*, 943–951.
- Barlowe, C. (2010). ER sheets get roughed up. *Cell* *143*, 665–666.
- Barral, Y., Parra, M., Bidlingmaier, S., and Snyder, M. (1999). Nim1-related kinases coordinate cell cycle progression with the organization of the peripheral cytoskeleton in yeast. *Genes Dev.* *13*, 176–187.
- Bechmann, L.P., Hannivoort, R.A., Gerken, G., Hotamisligil, G.S., Trauner, M., and Canbay, A. (2012). The interaction of hepatic lipid and glucose metabolism in liver diseases. *J. Hepatol.* *56*, 952–964.
- Bi, E., Maddox, P., Lew, D.J., Salmon, E.D., McMillan, J.N., Yeh, E., and Pringle, J.R. (1998). Involvement of an actomyosin contractile ring in *Saccharomyces cerevisiae* cytokinesis. *J. Cell Biol.* *142*, 1301–1312.
- Bos, J.L., Rehmann, H., and Wittinghofer, A. (2007). GEFs and GAPs: critical elements in the control of small G proteins. *Cell* *129*, 865–877.
- Caudron, F., and Barral, Y. (2009). Septins and the lateral compartmentalization of eukaryotic membranes. *Dev. Cell* *16*, 493–506.
- Chao, J.T., Wong, A.K., Tavassoli, S., Young, B.P., Chruscicki, A., Fang, N.N., Howe, L.J., Mayor, T., Foster, L.J., and Loewen, C.J. (2014). Polarization of the endoplasmic reticulum by ER-septin tethering. *Cell* *158*, 620–632.
- Chen, C.T., Ettinger, A.W., Huttner, W.B., and Doxsey, S.J. (2013). Resurrecting remnants: the lives of post-mitotic midbodies. *Trends Cell Biol.* *23*, 118–128.
- Chen, H., Howell, A.S., Robeson, A., and Lew, D.J. (2011). Dynamics of septin ring and collar formation in *Saccharomyces cerevisiae*. *Biol. Chem.* *392*, 689–697.

- Chen, R.E., and Thorner, J. (2007). Function and regulation in MAPK signaling pathways: lessons learned from the yeast *Saccharomyces cerevisiae*. *Biochim. Biophys. Acta* *1773*, 1311–1340.
- Costanzo, M., Baryshnikova, A., Myers, C.L., Andrews, B., and Boone, C. (2011). Charting the genetic interaction map of a cell. *Curr. Opin. Biotechnol.* *22*, 66–74.
- Denic, V., Quan, E.M., and Weissman, J.S. (2006). A luminal surveillance complex that selects misfolded glycoproteins for ER-associated degradation. *Cell* *126*, 349–359.
- Du, Y., Ferro-Novick, S., and Novick, P. (2004). Dynamics and inheritance of the endoplasmic reticulum. *J. Cell Sci.* *117*, 2871–2878.
- Erjavec, N., Larsson, L., Grantham, J., and Nyström, T. (2007). Accelerated aging and failure to segregate damaged proteins in Sir2 mutants can be suppressed by overproducing the protein aggregation-remodeling factor Hsp104p. *Genes Dev.* *21*, 2410–2421.
- Ettinger, A.W., Wilsch-Bräuninger, M., Marzesco, A.M., Bickle, M., Lohmann, A., Maliga, Z., Karbanová, J., Corbeil, D., Hyman, A.A., and Huttner, W.B. (2011). Proliferating versus differentiating stem and cancer cells exhibit distinct midbody-release behaviour. *Nat. Commun.* *2*, 503.
- Fehrenbacher, K.L., Davis, D., Wu, M., Boldogh, I., and Pon, L.A. (2002). Endoplasmic reticulum dynamics, inheritance, and cytoskeletal interactions in budding yeast. *Mol. Biol. Cell* *13*, 854–865.
- Feige, M.J., and Hendershot, L.M. (2011). Disulfide bonds in ER protein folding and homeostasis. *Curr. Opin. Cell Biol.* *23*, 167–175.
- Field, C.M., and Kellogg, D. (1999). Septins: cytoskeletal polymers or signalling GTPases? *Trends Cell Biol.* *9*, 387–394.
- Finnigan, G.C., Takagi, J., Cho, C., and Thorner, J. (2015). Comprehensive genetic analysis of paralogous terminal septin subunits Shs1 and Cdc11 in *Saccharomyces cerevisiae*. *Genetics* *200*, 821–841.
- Frakes, A.E., and Dillin, A. (2017). The UPRER: sensor and coordinator of organismal homeostasis. *Mol. Cell* *66*, 761–771.
- Frand, A.R., and Kaiser, C.A. (1998). The ERO1 gene of yeast is required for oxidation of protein dithiols in the endoplasmic reticulum. *Mol. Cell* *1*, 161–170.
- Gladfelter, A.S., Pringle, J.R., and Lew, D.J. (2001). The septin cortex at the yeast mother-bud neck. *Curr. Opin. Microbiol.* *4*, 681–689.
- Gustin, M.C., Albertyn, J., Alexander, M., and Davenport, K. (1998). MAP kinase pathways in the yeast *Saccharomyces cerevisiae*. *Microbiol. Mol. Biol. Rev.* *62*, 1264–1300.
- Hansen, A.S., Hao, N., and O’Shea, E.K. (2015). High-throughput microfluidics to control and measure signaling dynamics in single yeast cells. *Nat. Protoc.* *10*, 1181–1197.
- Hartwell, L.H. (1974). *Saccharomyces cerevisiae* cell cycle. *Bacteriol. Rev.* *38*, 164–198.
- Hereford, L.M., and Hartwell, L.H. (1974). Sequential gene function in the initiation of *Saccharomyces cerevisiae* DNA synthesis. *J. Mol. Biol.* *84*, 445–461.
- Higuchi-Sanabria, R., Pernice, W.M., Vevea, J.D., Alessi Wolken, D.M., Boldogh, I.R., and Pon, L.A. (2014). Role of asymmetric cell division in lifespan control in *Saccharomyces cerevisiae*. *FEMS Yeast Res.* *14*, 1133–1146.
- Kang, P.J., Sanson, A., Lee, B., and Park, H.O. (2001). A GDP/GTP exchange factor involved in linking a spatial landmark to cell polarity. *Science* *292*, 1376–1378.
- Kono, K., Saeki, Y., Yoshida, S., Tanaka, K., and Pellman, D. (2012). Proteasomal degradation resolves competition between cell polarization and cellular wound healing. *Cell* *150*, 151–164.
- Kozubowski, L., Saito, K., Johnson, J.M., Howell, A.S., Zyla, T.R., and Lew, D.J. (2008). Symmetry-breaking polarization driven by a Cdc42p GEF-PAK complex. *Curr. Biol.* *18*, 1719–1726.
- Kuo, S.C., and Lampen, J.O. (1974). Tunicamycin—an inhibitor of yeast glycoprotein synthesis. *Biochem. Biophys. Res. Commun.* *58*, 287–295.
- Kuo, T.C., Chen, C.T., Baron, D., Onder, T.T., Loewer, S., Almeida, S., Weismann, C.M., Xu, P., Houghton, J.M., Gao, F.B., et al. (2011). Midbody accumulation through evasion of autophagy contributes to cellular reprogramming and tumorigenicity. *Nat. Cell Biol.* *13*, 1214–1223.
- Li, X., Du, Y., Siegel, S., Ferro-Novick, S., and Novick, P. (2010). Activation of the mitogen-activated protein kinase, Sit2p, at bud tips blocks a late stage of endoplasmic reticulum inheritance in *Saccharomyces cerevisiae*. *Mol. Biol. Cell* *21*, 1772–1782.
- Lippincott, J., and Li, R. (1998). Dual function of Cyk2, a cdc15/PSTPIP family protein, in regulating actomyosin ring dynamics and septin distribution. *J. Cell Biol.* *143*, 1947–1960.
- Liu, D., and Novick, P. (2014). Bem1p contributes to secretory pathway polarization through a direct interaction with Exo70p. *J. Cell Biol.* *207*, 59–72.
- Lord, M., Laves, E., and Pollard, T.D. (2005). Cytokinesis depends on the motor domains of myosin-II in fission yeast but not in budding yeast. *Mol. Biol. Cell* *16*, 5346–5355.
- Madden, K., and Snyder, M. (1998). Cell polarity and morphogenesis in budding yeast. *Annu. Rev. Microbiol.* *52*, 687–744.
- Marston, A.L., Chen, T., Yang, M.C., Belhumeur, P., and Chant, J. (2001). A localized GTPase exchange factor, Bud5, determines the orientation of division axes in yeast. *Curr. Biol.* *11*, 803–807.
- Meitinger, F., Khmelinskii, A., Morlot, S., Kurtulmus, B., Palani, S., Andres-Pons, A., Hub, B., Knop, M., Charvin, G., and Pereira, G. (2014). A memory system of negative polarity cues prevents replicative aging. *Cell* *159*, 1056–1069.
- Mori, K. (2000). Tripartite management of unfolded proteins in the endoplasmic reticulum. *Cell* *101*, 451–454.
- Mostowy, S., and Cossart, P. (2012). Septins: the fourth component of the cytoskeleton. *Nat. Rev. Mol. Cell Biol.* *13*, 183–194.
- Nelson, S.A., Sanson, A.M., Park, H.O., and Cooper, J.A. (2012). A novel role for the GTPase-activating protein Bud2 in the spindle position checkpoint. *PLoS One* *7*, e36127.
- Oh, Y., and Bi, E. (2011). Septin structure and function in yeast and beyond. *Trends Cell Biol.* *21*, 141–148.
- Okada, S., Leda, M., Hanna, J., Savage, N.S., Bi, E., and Goryachev, A.B. (2013). Daughter cell identity emerges from the interplay of Cdc42, septins, and exocytosis. *Dev. Cell* *26*, 148–161.
- Onishi, M., Ko, N., Nishihama, R., and Pringle, J.R. (2013). Distinct roles of Rho1, Cdc42, and Cyk3 in septum formation and abscission during yeast cytokinesis. *J. Cell Biol.* *202*, 311–329.
- Park, H.O., Bi, E., Pringle, J.R., and Herskowitz, I. (1997). Two active states of the Ras-related Bud1/Rsr1 protein bind to different effectors to determine yeast cell polarity. *Proc. Natl. Acad. Sci. USA* *94*, 4463–4468.
- Park, H.O., Kang, P.J., and Rachfal, A.W. (2002). Localization of the Rsr1/Bud1 GTPase involved in selection of a proper growth site in yeast. *J. Biol. Chem.* *277*, 26721–26724.
- Piña, F., Yagisawa, F., Obara, K., Gregerson, J.D., Kihara, A., and Niwa, M. (2018). Sphingolipids activate the endoplasmic reticulum stress surveillance pathway. *J. Cell Biol.* *217*, 495–505.
- Piña, F.J., Fleming, T., Pogliano, K., and Niwa, M. (2016). Reticulons regulate the ER inheritance block during ER stress. *Dev. Cell* *37*, 279–288.
- Piña, F.J., and Niwa, M. (2015). The ER Stress Surveillance (ERSU) pathway regulates daughter cell ER protein aggregate inheritance. *ELife* *4*.
- Pohl, C., and Jentsch, S. (2009). Midbody ring disposal by autophagy is a post-abscission event of cytokinesis. *Nat. Cell Biol.* *11*, 65–70.
- Pollard, M.G., Travers, K.J., and Weissman, J.S. (1998). Ero1p: a novel and ubiquitous protein with an essential role in oxidative protein folding in the endoplasmic reticulum. *Mol. Cell* *1*, 171–182.
- Powell, C.D., Quain, D.E., and Smart, K.A. (2003). Chitin scar breaks in aged *Saccharomyces cerevisiae*. *Microbiology (Reading, Engl.)* *149*, 3129–3137.
- Pruyne, D., and Bretscher, A. (2000). Polarization of cell growth in yeast. I. Establishment and maintenance of polarity states. *J. Cell Sci.* *113*, 365–375.
- Pruyne, D., Legesse-Miller, A., Gao, L., Dong, Y., and Bretscher, A. (2004). Mechanisms of polarized growth and organelle segregation in yeast. *Annu. Rev. Cell Dev. Biol.* *20*, 559–591.
- Robinson, M.D., Grigull, J., Mohammad, N., and Hughes, T.R. (2002). FunSpec: a web-based cluster interpreter for yeast. *BMC Bioinformatics* *3*, 35.

- Ron, D., and Walter, P. (2007). Signal integration in the endoplasmic reticulum unfolded protein response. *Nat. Rev. Mol. Cell Biol.* 8, 519–529.
- Rutkowski, D.T., and Kaufman, R.J. (2004). A trip to the ER: coping with stress. *Trends Cell Biol.* 14, 20–28.
- Schmidt, M., Bowers, B., Varma, A., Roh, D.H., and Cabib, E. (2002). In budding yeast, contraction of the actomyosin ring and formation of the primary septum at cytokinesis depend on each other. *J. Cell Sci.* 115, 293–302.
- Shcheprova, Z., Baldi, S., Frei, S.B., Gonnet, G., and Barral, Y. (2008). A mechanism for asymmetric segregation of age during yeast budding. *Nature* 454, 728–734.
- Sheff, M.A., and Thorn, K.S. (2004). Optimized cassettes for fluorescent protein tagging in *Saccharomyces cerevisiae*. *Yeast* 21, 661–670.
- Sheu, Y.J., Santos, B., Fortin, N., Costigan, C., and Snyder, M. (1998). Spa2p interacts with cell polarity proteins and signaling components involved in yeast cell morphogenesis. *Mol. Cell Biol.* 18, 4053–4069.
- Sinclair, D.A., Mills, K., and Guarente, L. (1998). Molecular mechanisms of yeast aging. *Trends Biochem. Sci.* 23, 131–134.
- Singh, P., Ramachandran, S.K., Zhu, J., Kim, B.C., Biswas, D., Ha, T., Iglesias, P.A., and Li, R. (2017). Sphingolipids facilitate age asymmetry of membrane proteins in dividing yeast cells. *Mol. Biol. Cell* 28, 2712–2722.
- Smith, S.E., Rubinstein, B., Mendes Pinto, I., Slaughter, B.D., Unruh, J.R., and Li, R. (2013). Independence of symmetry breaking on Bem1-mediated autocatalytic activation of Cdc42. *J. Cell Biol.* 202, 1091–1106.
- Spokoini, R., Moldavski, O., Nahmias, Y., England, J.L., Schuldiner, M., and Kaganovich, D. (2012). Confinement to organelle-associated inclusion structures mediates asymmetric inheritance of aggregated protein in budding yeast. *Cell Rep.* 2, 738–747.
- Tarassov, K., Messier, V., Landry, C.R., Radinovic, S., Serna Molina, M.M., Shames, I., Malitskaya, Y., Vogel, J., Bussey, H., and Michnick, S.W. (2008). An in vivo map of the yeast protein interactome. *Science* 320, 1465–1470.
- Thieleke-Matos, C., Osório, D.S., Carvalho, A.X., and Morais-de-Sá, E. (2017). Emerging mechanisms and roles for asymmetric cytokinesis. *Int. Rev. Cell Mol. Biol.* 332, 297–345.
- Toenjes, K.A., Simpson, D., and Johnson, D.I. (2004). Separate membrane targeting and anchoring domains function in the localization of the *S. cerevisiae* Cdc24p guanine nucleotide exchange factor. *Curr. Genet.* 45, 257–264.
- Tolliday, N., Pitcher, M., and Li, R. (2003). Direct evidence for a critical role of myosin II in budding yeast cytokinesis and the evolvability of new cytokinetic mechanisms in the absence of myosin II. *Mol. Biol. Cell* 14, 798–809.
- Tong, A.H., and Boone, C. (2006). Synthetic genetic array analysis in *Saccharomyces cerevisiae*. *Methods Mol. Biol.* 313, 171–192.
- Tu, B.P., Ho-Schleyer, S.C., Travers, K.J., and Weissman, J.S. (2000). Biochemical basis of oxidative protein folding in the endoplasmic reticulum. *Science* 290, 1571–1574.
- van Drogen, F., and Peter, M. (2002). Spa2p functions as a scaffold-like protein to recruit the Mpk1p MAP kinase module to sites of polarized growth. *Curr. Biol.* 12, 1698–1703.
- Verselle, M., and Thorner, J. (2004). Septin collar formation in budding yeast requires GTP binding and direct phosphorylation by the PAK, Cla4. *J. Cell Biol.* 164, 701–715.
- Verselle, M., and Thorner, J. (2005). Some assembly required: yeast septins provide the instruction manual. *Trends Cell Biol.* 15, 414–424.
- Voth, W.P., Olsen, A.E., Sbia, M., Freedman, K.H., and Stillman, D.J. (2005). ACE2, CBK1, and BUD4 in budding and cell separation. *Eukaryot. Cell* 4, 1018–1028.
- Watts, F.Z., Shiels, G., and Orr, E. (1987). The yeast MYO1 gene encoding a myosin-like protein required for cell division. *EMBO J.* 6, 3499–3505.
- Weirich, C.S., Erzberger, J.P., and Barral, Y. (2008). The septin family of GTPases: architecture and dynamics. *Nat. Rev. Mol. Cell Biol.* 9, 478–489.
- Weiss, E.L. (2012). Mitotic exit and separation of mother and daughter cells. *Genetics* 192, 1165–1202.
- Westrate, L.M., Lee, J.E., Prinz, W.A., and Voeltz, G.K. (2015). Form follows function: the importance of endoplasmic reticulum shape. *Annu Rev Biochem* 84, 791–811.
- Wloka, C., and Bi, E. (2012). Mechanisms of cytokinesis in budding yeast. *Cytoskeleton (Hoboken)* 69, 710–726.
- Wu, C.F., Chiou, J.G., Minakova, M., Woods, B., Tsygankov, D., Zyla, T.R., Savage, N.S., Elston, T.C., and Lew, D.J. (2015). Role of competition between polarity sites in establishing a unique front. *ELife* 4.
- Wu, N., Sarna, L.K., Hwang, S.Y., Zhu, Q., Wang, P., Siow, Y.L., and O, K. (2013). Activation of 3-hydroxy-3-methylglutaryl coenzyme A (HMG-CoA) reductase during high fat diet feeding. *Biochim. Biophys. Acta* 1832, 1560–1568.
- Young, B.P., and Loewen, C.J. (2013). Balony: a software package for analysis of data generated by synthetic genetic array experiments. *BMC Bioinformatics* 14, 354.

## STAR★METHODS

### KEY RESOURCES TABLE

REAGENT or RESOURCE	SOURCE	IDENTIFIER
<b>Antibodies</b>		
Anti-GFP Mouse Monoclonal (No Longer Available)	Roche	11814460001
Anti-Myc Mouse Monoclonal	Sigma	M4439
Anti-PGK1 Mouse Monoclonal	Invitrogen	459250
<b>Chemicals, Peptides, and Recombinant Proteins</b>		
GFP-nAb Magnetic Agarose Beads	Allele Biotech	ABP-NAB-GFPXK20
Protease Inhibitor Cocktail	Sigma	P8215
Concanavalin A	Sigma	C2010
Calcofluor White	Sigma	18909
Wheat Germ Agglutinin, Alexa Fluor 555 Conjugate	Invitrogen	W32464
ML 141	Sigma	SML0407
Tunicamycin	Calbiochem	CAS 11089-65-9
<b>Experimental Models: Organisms/Strains</b>		
See <a href="#">Table S5</a>	N/A	N/A
<b>Oligonucleotides</b>		
See <a href="#">Table S4</a>	N/A	N/A
<b>Recombinant DNA</b>		
P4339	Boone lab, U of Toronto	N/A
pHVf1CT	Loewen lab, UBC	<a href="#">Chao et al., 2014</a>
pUVf2CT	Loewen lab, UBC	<a href="#">Chao et al., 2014</a>
Ylp211-GIC2PBD(W23A)-RFP	Bi lab, U of Pennsylvania	N/A
316>GIC2-PBD-RFP	this paper	N/A
416-TEF>BUD2	this paper	N/A
416-TEF>BUD5	this paper	N/A
416-TEF>SHS1	this paper	N/A
pKT128	<a href="#">Sheff and Thorn, 2004</a>	N/A
pFA6A-pmRFP-KanMX6	<a href="#">Bähler et al., 1998</a>	N/A
pFA6A-13Myc-KanMX6		
<b>Software and Algorithms</b>		
ImageJ	NIH	N/A
Prism 5.0	GraphPad	N/A
Cytoscape 3.2	N/A	N/A
<b>Strains</b>		
Name	Genotype	Source
BY4741	MATa his3Δ1 leu2Δ0 met15Δ0 ura3Δ0	This lab
BY7092	MATalpha can1delta::STE2pr-Sp_his5 lyp1delta his3delta1 leu2delta0 ura3delta0 met15delta0	Boone lab
BY7043	MATalpha can1Δ::STE2pr-lue2 lyp1Δ his3Δ 1 leu2Δ0 ura3Δ0 met15Δ0	Boone lab
MNY1032	SHS1-GFP::KanMX W303 background	This lab
MNY2434	UPRE-GFP::URA in ABY100	This lab
MNY2659	Nba1-GFP::HIS in BY 7043	This lab
MNY2660	Pho88-GFP::HIS in BY 7043	This lab

(Continued on next page)

**Continued**

Strains

Name	Genotype	Source
MNY2660	Pho88-GFP::HIS in BY 7043	This lab
MNY2662	Shs1-GFP::HIS in BY 7043	This lab
MNY2663	Shs1-cte-GFP::HIS in BY 7043	This lab
MNY2664	Cdc11-GFP::HIS in BY 4741	This lab
MNY2669	shs1-cte::NAT in BY7092	This lab
MNY2671	$\Delta$ slt2::NAT in BY7092	This lab
MNY2672	$\Delta$ nba1::NAT in BY7092	This lab
MNY2685	$\Delta$ slt2::KanMX Shs1-GFP::HIS	This lab
MNY2687	$\Delta$ nba1::KanMX Shs1-GFP::HIS	This lab
MNY2689	$\Delta$ nba1::NAT $\Delta$ ice2::KanMX	This lab
MNY2690	$\Delta$ slt2::NAT $\Delta$ nba1::KanMX	This lab
MNY2691	$\Delta$ slt2::KanMX shs1-cte::NAT by tetrad (MAT a)	This lab
MNY2700	Shs1-RFP::KanMX X Nba1-GFP::HIS	This lab
MNY2718	Shs1-RFP::KanMX Myo1-GFP::HIS	This lab
MNY2724	ero1-1::KanMX Shs1-GFP::HIS	This lab
MNY2785	Bud2-GFP::HIS BY7043	This lab
MNY2788	Bud5-GFP::HIS BY7043	This lab
MNY2789	Shs1-VF1::HIS in 4741	This lab
MNY2790	VF1-Slt2::HIS in 4741	This lab
MNY2794	Nba1-VF2::URA BY 7043	This lab
MNY2815	$\Delta$ slt2::KanMX shs1-cte::NAT Pho88-GFP::HIS	This lab
MNY2816	$\Delta$ slt2::KanMX shs1-cte::NAT Cdc11-GFP::HIS	This lab
MNY2817	$\Delta$ slt2::NAT Pho88-GFP::HIS	This lab
MNY2818	shs1-cte::NAT Pho88-GFP::HIS	This lab
MNY2830	Bud1-VF1::HIS Cdc24-VF2::URA	This lab
MNY2832	Bud1-VF1::HIS in 4741	This lab
MNY2833	Bud2-VF2::URA in 7043	This lab
MNY2834	Bud5-VF2::URA in 7043	This lab
MNY2835	Cdc24-VF2::URA in 7043	This lab
MNY2836	Bem1-VF2::URA in 7043	This lab
MNY2840	Bud5-GFP::HIS $\Delta$ slt2::KanMX shs1-cte::NAT	This lab
MNY2841	Cdc24-GFP::HIS $\Delta$ slt2::G418 shs1-cte::NAT	This lab
MNY2850	Bud2-GFP::HIS shs1-cte::NAT	This lab
MNY2851	Bud5-GFP::HIS shs1-cte::NAT	This lab
MNY2852	Cdc24-GFP::HIS shs1-cte::NAT	This lab
MNY2853	Cdc24-GFP::HIS $\Delta$ slt2::KanMX	This lab
MNY2854	Bud5-GFP::HIS $\Delta$ slt2::G418	This lab
MNY2856	Slt2-13myc::KanMX 4741	This lab
MNY2857	Shs1-13myc::KanMX 4741	This lab
MNY2858	Bud2-GFP::HIS $\Delta$ slt2::KanMX	This lab
MNY2859	Bem1-GFP::HIS 7043	This lab
MNY2879	Shs1-GFP::HIS $\Delta$ bem1::KanMX	This lab
MNY2881	Shs1-GFP::HIS $\Delta$ rax1::KanMX	This lab
MNY2890	316>Gic2-PBD-RFP in 4741	This lab
MNY2891	Cdc24-GFP::HIS 7043	This lab
MNY2828	Bud1-VF1::HIS x Bud2-VF2::URA	This lab

(Continued on next page)

**Continued**

Strains		
Name	Genotype	Source
MNY2829	Bud1-VF1::HIS x Bud5-VF2::URA	This lab
MNY2831	VF1-Slt2::HIS x Bem1-VF2::URA	This lab
Primers		
oligo Name	Sequence 5'–3'	
Δslt2_KO_F'	tagaaataattgaaggcgtgtataacaattctgggagACATGGAGGCC	
Δslt2_KO_R'	ggtgattctatactccccggttacttatagttttgCAGTATAGCGACCAGCATTAC	
Δslt2_Ko_Chk_F'	CCTGTGTGTAGTGAAAAATTCGAAT	
Δslt2_Ko_Chk_R'	ctatggtgattctatactccccg	
Nba1_KO_F	atatcgactaacaagaagaccattatcaaaaccagatACATGGAGGCCAGAATACCCT	
Nba1_KO_R	ACCGGAAGAGAAAAGAACTTATATATTACCATACTcagtatagcgaccagcattcac	
Nba1_Chk_F	CCACAGTTAGTGAACAAAA	
Nba1_Chk_R	GCTTTGTCTAATCTTTTCAG	
Sec63-GFP_KI_F	ATCGATACGGATACAGAAGCTGAAGATGATGAATCACCAGAAGGTgacgg	
Sec63-GFP_KI_R	cgctaaagactaaaatgaaaactataactcattatTCGatgaattcgagctcg	
Shs1-CTE KO_F	CACCACGCAAAATTTGCTTTACGAGAATTACCGTTCCGACATGGAGGCCAGAATACCCT	
Shs1-CTE KO_R	gctttgattttgtacagatacaacTCAATCTTACCCAGTATAGCGACCAGCATTAC	
Shs1_KO_Chk_F	CCACGCAAAATTTGCTTTACG	
Shs1_KO_Chk_R	CGATGCAATAGAGGCTAAATC	
Shs1-GFP_KI_F	GACACGTATACTGATTTAGCCTCTATTGCATCGGGTAGAGATGGTgacggtgctggttta	
Shs1-GFP_KI_R	tatttattattgtcagctttggattttgtacagatacaTCGatgaattcgagctcg	
Shs1ΔCTE_GFP_F	AAACTATCGTCCGTGGCCAACGCTGAAGAAATTTGGTCTAATGGTgacggtgctggttta	
Pho88-GFP_KI_F	GAAGAAGCTGAAAGAGCCGGTAACGCTGGTGAAGGCTGAAGGTgacgg	
Pho88-GFP_KI_R	gcagcaactgcgtagagaaaaaatgaatattttacataTCGatgaattcgagctcg	
Pho88-RFP-KI-F	AGAAGCTGAAAGAGCCGGTAACGCTGGTGAAGGCTGAACGGATCCCCGGTTAATTA	
Pho88-RFP-KI-R	gcagcaactgcgtagagaaaaaatgaatattttacaGAATTCGAGCTCGTTAAAC	
Shs1-RFP-KI-F	CACGTATACTGATTTAGCCTCTATTGCATCGGGTAGAGATCGGATCCCCGGTTAATTA	
Shs1-RFP-KI-R	tatttattattgtcagctttggattttgtacagatacaGAATTCGAGCTCGTTAAAC	
Cdc11-GFP_KI_F	GAAGCCAGGTTGAAAAAGAGGCGAAAAATCAAACAGGAAGAAGGTgacggtgctggttta	
Cdc11-GFP_KI_R	atatagagaagaagaataagtgagggaagcgaagcggacTCGatgaattcgagctcg	
VF1_R_Chk	CATTAACATCACCATCTAATTCAACC	
VF2_R_Chk	ACCACCATCTCAATGTTGTGTC	
Nba1-VF-KI_F	GATTAGACAAAGCTACAAAGGCTCTTGAAGGTTTatgtatcacacacacagattag	
Nba1-VF-KI_R	CGGACTTGTCCAAGTATCAATGAATACAAGCCATTGAATTACtcatgaattcgagctcg	
Myo1-GFP_F	AAAAATATTGATAGTAACAATGCACAGAGTAAATTTTCAGTGGTgacggtgctggttta	
Myo1-GFP_R	cggtgctctttttctgtaataatgcattctcattctgtTCGatgaattcgagctcg	
Shs1-VF1/2 KI_F	TAGCCTCTATTGCATCGGGTAGAGATggtgctggttatgtatcacacacacagattag	
Shs1-VF1/2 KI_R	atttattattgtcagctttggattttgtacagatacaactcgatgaattcgagctcg	
Bud2-GFP_KI_F	CTGACAAGATGGTTCAAAAAGAAAAAGAAACAGGGGGATCTGGTgacggtgctggttta	
Bud2-GFP_KI_R	cttcaaggaagaatgaagtgaaacatttttctacgaTCGatgaattcgagctcg	
Bud5-GFP_KI_F	AGGGCGTATCAAGTCAGTATAGCTAAGGTTCCAAGGCTTACCGGTgacggtgctggttta	
Bud5-GFP_KI_R	aagaagcaaaaggaagtcattcttcttgaacagttctgtttTCGatgaattcgagctcg	
Cdc24-GFP_F	TTGGCGAAAACAATGAGAAATCTTGAACATTCGTCTGTATGGTgacggtgctggttta	
Cdc24-GFP_R	ttctgattatttagtattgtctatactagttttatTCGatgaattcgagctcg	
Bud5_KO_F	gacctctgagcggtagcctctggcaagaagaagaACATGGAGGCCAGAATACCCT	
Bud5_KO_R	agcaaaaggaagtcattcttcttgaacagttctgtttCAGTATAGCGACCAGCATTAC	
Bud5_KO_Chk_F	ACTGACCTCAGTGATTTACTTTTCC	
Bud5_KO_Chk_R	GCAGTGATGTAAGGTACACAAGG	
Bud2_KO_F	gcatacgtcgtggtttatcttggattgtatcatattACATGGAGGCCAGAATACCCT	

(Continued on next page)

**Continued**

Primers	
oligo Name	Sequence 5'–3'
Bud2_KO_R	tcaaaggaagaatatgaagtgaacattttttctacgCAGTATAGCGACCAGCATTAC
Bud2_KO_Chk_R	tattccacattctggatcgc
Bud5-VF Ki F	ATCAAGTCAGTATAGCTAAGGTTCCAAGGCTTACctatgtatcacacacacacgatttag
Bud2-VF Ki F	GATGGTTCAAAAAGAAAAAGAAACAGGGGGATCTatgtatcacacacacacgatttag
Cdc24-VF Ki F	AAAACAATGAGAAATTCCTGAACATTCGTCTGTATatgtatcacacacacacgatttag
Bud1-VF Ki F	AAAGAAGAAAAACGCTTCCACTTGCCTATTCTAtatgtatcacacacacacgatttag
Bud1-VF Ki R	ttttatctgatcttgattcattataataaaaattaagtgtatcgatgaattcgagctcg
Bem1-GFP_F	AACATAATCCAAGCCAAACTGAAAATTTCCGTTACGATATTGGTgacggtgctggttta
New Bem1-VF_R	aaagaagaaaaatgctctgtcttaacactagatactagattcgatgaattcgagctcg
Bud3_KO_Chk_F	GACAAAGAGAACGATGAAACC
Bud3_KO_Chk_R	CCTGATGTAAAGAAGCGCTTC
Bud4_KO_Chk_F	AGGAGATAGACAATGAAATGG
Bud4_KO_Chk_R	GCATCTTCTCCTCTTCATCT
new_Bud2_cloning_F	cccggggtcgacATGAGCTCCAACAATGAACCGGCC
new_Bud2_cloning_R	cccggggaattccgaTTAAGATCCCCCTGTTTCTTTT
XbaI-Bud2_F	gcgctctagaATGAGCTCCAACAATGAACC
Bud2-Sall_R	ggccgtcgaccgaTTAAGATCCCCCTGTTT
XbaI-Shs1_F	gcgctctagaATGAGCACTGCTTCAACACC
Shs1-Sall_R	ggccgtcgacTCAATCTCTACCCGATGCAA
Gic2PBD-RFP_F	ccccgagctcgatctagatgttgc
Gic2PBD-RFP_R	ccagtgatcggagctcGGTACC
Slt2-13Myc-KI_F	TGAAAAAGAGCTGGAGTTTGGATTAGATAGAAAATATTTTCGGATCCCCGGGTTAATTA
Slt2-13Myc-KI_R	gggtattctatactccccggttacttatagttttgtcGAATTTCGAGCTCGTTAAAC

**LEAD CONTACT AND MATERIALS AVAILABILITY**

Further information and requests for resources and reagents should be directed to and will be fulfilled by the Lead Contact, Maho Niwa ([mniwarosen@ucsd.edu](mailto:mniwarosen@ucsd.edu)).

**EXPERIMENTAL MODEL AND SUBJECT DETAILS**

Unless otherwise indicated, all yeast strains used in this study is of the S288C background. See [Table S5](#) for a full list of strains. All yeast was grown at 30°C in synthetic defined medium containing yeast nitrogenous base, 2% dextrose and the appropriate amino acids for the genotype unless otherwise stated.

**METHOD DETAILS**

**Plasmid Construction**

Epitope-tagging of endogenous proteins was done by homologous recombination of PCR-generated fragments from templates in haploids at the C-terminus of the specified genes at their endogenous locus in either BY7043 ([Tong and Boone, 2006](#)) or BY4741. The templates include pKT128 (GFP::SpHIS5) ([Sheff and Thorn, 2004](#)), pFA6A-pmRFP-KanMX6, pFA6A-13Myc-KanMX6 ([Bähler et al., 1998](#)), pHVF1CT and pUVF2CT ([Chao et al., 2014](#)). KanMX deletion strains were obtained from freezer stocks of the haploid yeast deletion collection (BY4741, MAT a, KanMX; Thermo Fischer). NatR deletion or truncation strains were constructed in BY7092 using p4339 ([Tong and Boone, 2006](#)). All deletion and truncation strains were confirmed by PCR. Double epitope tagged (including, GFP/RFP) and double deletion strains were generated by standard yeast genetic techniques of sporulation and tetrad dissection. Split-YFP PCA strain construction was done as described in ([Chao et al., 2014](#)). For the expression of *BUD2*, *BUD5* and *SHS1*, full-length ORFs were cloned from BY4741 genomic DNA and inserted into p416-TEF at XbaI/Sall. To create p316-Gic2-PBD-RFP, *Gic2prom>Gic2-PBD-RFP* was PCR-cloned from YIp211-GIC2PBD(W23A)-RFP into pRS316 plasmid at XbaI/ KpnI.

**Light Microscopy techniques**

Log phase live yeast cells were imaged using the Zeiss Axiovert 200M with a 100×1.3 NA objective, or the DeltaVision system (Applied Precision) consisting of an inverted epifluorescence microscope (IX71, Olympus).

All time-lapse imaging was done using in-house fabricated microfluidics devices except for ER stress recovery experiments, in which we immobilized cells 1.6% agarose pads containing SC medium. For microfluidics, cells were immobilized in a microfluidic chamber using concanavalin A prepared at 2mg/ml with 50mM CaCl<sub>2</sub> and 50mM MnCl<sub>2</sub>. Microfluidics devices were fabricated exactly as described in (Hansen et al., 2015).

To visualize CRMs, we used either 0.1 μg/ml calcofluor white (Sigma) or Wheat Germ Agglutinin-555 conjugate as indicated. ER stress was induced by treating log-phase cultures with 1 μg/ml Tunicamycin for at least 1.5hr.

### Electron Microscopy

Transmission electron microscopy was performed as previously described (Onishi et al., 2013). Briefly, WT (W303) yeast cells were untreated or treated with 1 μg/ml Tunicamycin for 2 hrs at 30°C. The cells were harvested by filtration, fixed with 3% glutaraldehyde in 0.1 M sodium cacodylate buffer, pH 6.8, first for 1 h at RT, then at 4°C overnight. The fixed cells were washed three times with the same buffer, post-fixed with 4% potassium permanganate at 4°C for 2h, washed three times with H<sub>2</sub>O, incubated in 2% uranyl acetate at RT for 1h, washed twice with H<sub>2</sub>O, and dehydrated through a graded series of increasing ethanol concentrations. The cells were then embedded in LR white resin (Fluka; Sigma-Aldrich), and sections of ~70 nm were cut using a Leica Ultracut S microtome, collected on formvar-coated 100-mesh copper grids (Electron Microscopy Sciences), and post-stained for 30 sec in 1:1 3% uranyl acetate and 50% acetone, followed by 0.2% lead citrate for 3 min. Sections were then imaged at 120 kV using a JEM-1400 transmission electron microscope (JEOL) equipped with a Gatan Orius 4k X 4k digital camera.

### Split-DHFR Screen

Two libraries were employed for the DHFR PCA screen: a library with C-terminal DHFR F[1,2] tag and a library with C-terminal DHFR F[3] tag (Tarassov et al., 2008). A query strain was taken out from each library with Slit2 tagged with either fragment and mated against the opposite libraries by overnight incubation on YPD. After mating, diploid cells were selected for by incubation for 2 days on YPD medium with 100 μg/ml nourseothricin (Werner Bioagents) and 250 μg/ml hygromycin B (Wisent Bioproducts). This step was repeated once. Next, the strains were transferred to synthetic complete medium (4% (w/v) Noble agar) with 200 μg/ml methotrexate (Bioshop Canada) and without adenine or ammonium sulfate. Pictures of the strains were taken after 4 days incubation at 30°C. Colony size was analyzed using the Balony software (Young and Loewen, 2013).

### Co-purification Assays

Cells were harvested by centrifugation and resuspended with lysis buffer (20mM Tris-HCl, pH 7.4, 150mM NaCl, 1mM EDTA and 0.5% NP-40) containing protease inhibitor cocktail (Sigma) and bashed with acid-washed beads for 10min at 4°C. Cell lysates were homogenized by sonication. To purify GFP-tagged proteins, we used GFP-nAb magnetic agarose beads (Allele Biotech) and followed their recommended procedures. Purified proteins were confirmed by western blotting using anti-GFP antibody (Roche) at 1:1000, and co-purified binding partners by using anti-Myc antibody (Sigma) at 1:2000.

### Yeast Spot Assays

10- fold serial dilutions of log phase cells were spotted using a pin-frogger onto agar plates containing synthetic complete (SC) media with 2% glucose and grown for 48hr at 30°C.

### Quantification of Microscopy Images

The ImageJ software (National Institute of Health) was used for all quantifications, and a minimum of 100 cells was measured for each experiment. Progression through the cell cycle was arbitrarily classified as follows: G1, cells with no buds; S, bud area less than 1/3 of the mother; G2, bud area greater than 1/3, but less than 2/3 of the mother; and M phase, bud area greater than 2/3 of the mother. Bud to mother size ratios were determined by tracing bud and mother cell perimeters on the corresponding transmission images and measuring the area.

### Statistical Analysis

Statistical testing was performed using Graph Pad Prism (GraphPad Software). Experiments used for statistics were repeated 3 times. Quantitative data are expressed as mean ± SEM. Student's t test was used to generate *p* values.

### Gene-Set Enrichment Analysis for Split-DHFR Screen

The split-DHFR screen was analyzed by using FunSpec (Robinson et al., 2002). The resulting network was visualized using Cytoscape 3.2 using force-directed layout.

**Developmental Cell, Volume 51**

**Supplemental Information**

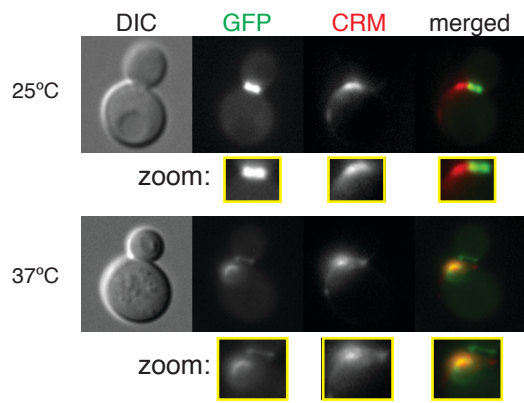
**Transfer of the Septin Ring to Cytokinetic**

**Remnants in ER Stress Directs Age-Sensitive**

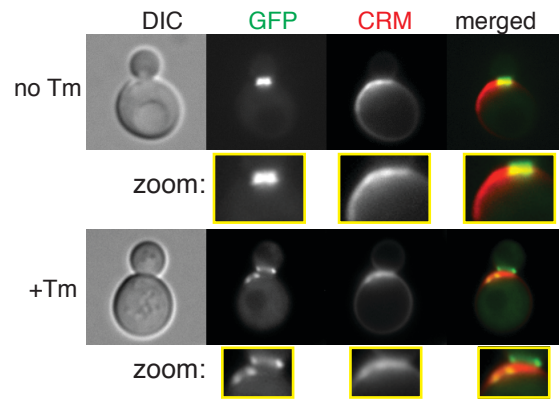
**Cell-Cycle Re-entry**

**Jesse T. Chao, Francisco Piña, Masayuki Onishi, Yifat Cohen, Ya-Shiuan Lai, Maya Schuldiner, and Maho Niwa**

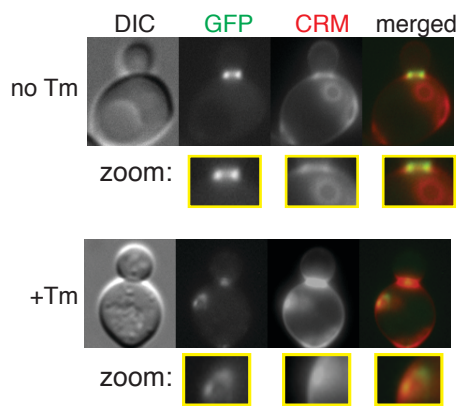
**A** Shs1-GFP, *ero1-1*



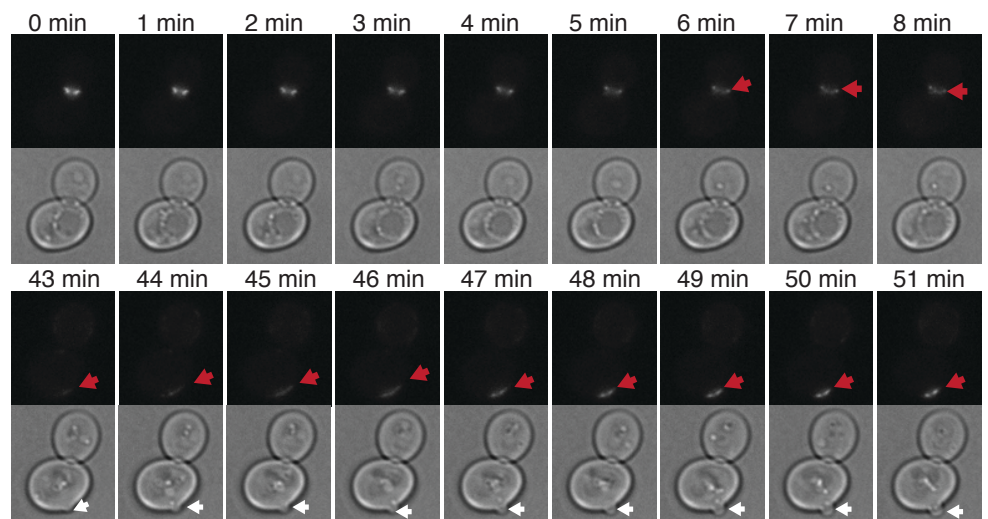
**B** Cdc11-GFP



**C** Shs1-GFP, W303 background



**D** Shs1-GFP, W303 background, no Tm



**E** Shs1-GFP, W303 background, + Tm

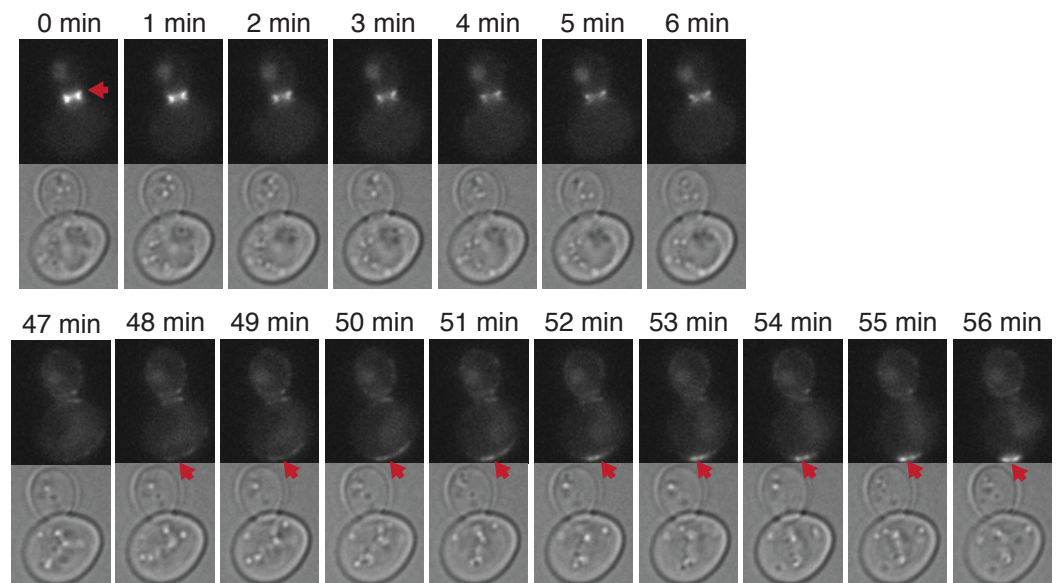
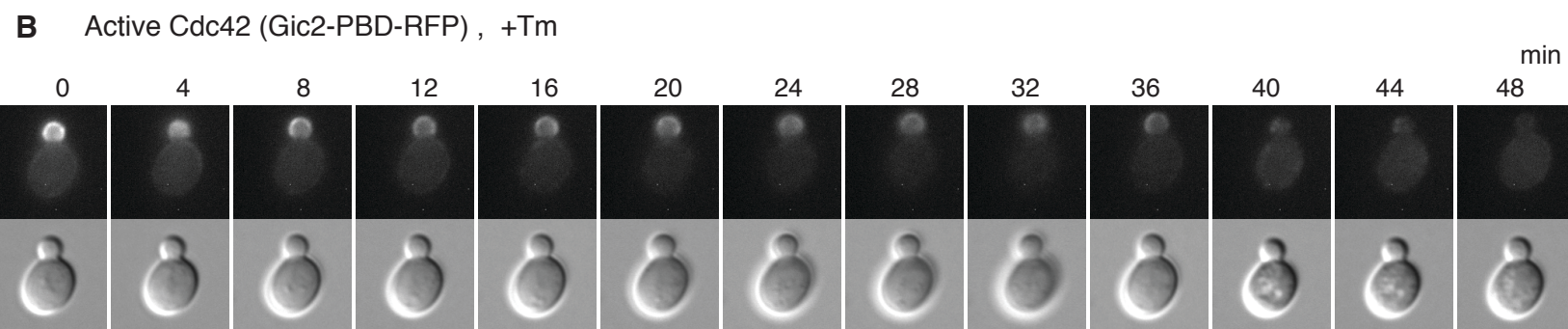
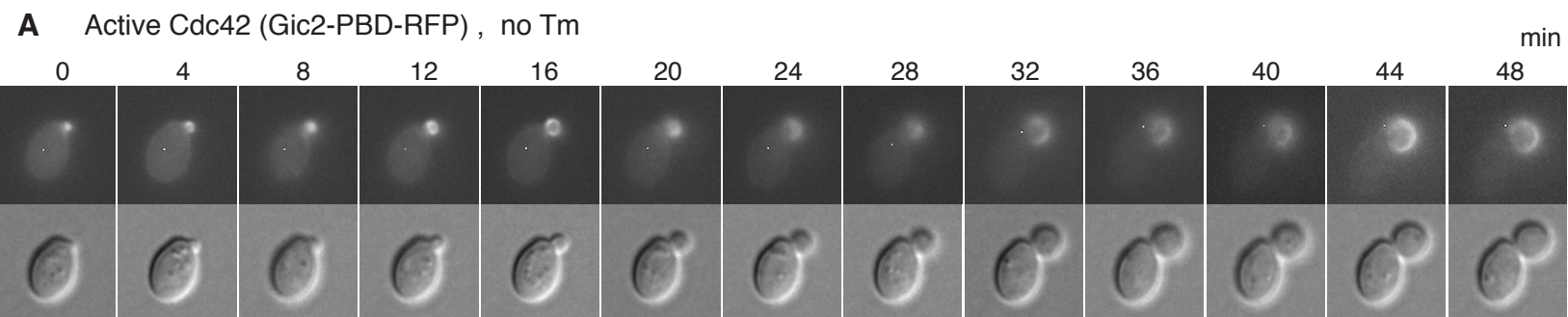


**Figure S1. Septin rings are mislocalized at CRMs regardless of ER stress types and of budding pattern differences. (Related to Figure 1)**

- (A) Shs1-GFP expressed in *ero1-1* cells grown at permissive (25°C) and non-permissive (37°C) temperatures. In all panels, zoomed images show cropped images from the bud neck regions, and CRMs were visualized by CWS.
- (B) Cdc11-GFP in WT cells grown without or with 1 µg/ml of Tm.
- (C) Shs1-GFP in WT cells of the W303 background grown without or with 1 µg/ml of Tm.
- (D and E) Time-lapse analysis of Shs1-GFP translocation in W303 cells either untreated (no Tm) (D) or treated with 1 µg/ml Tm (+Tm) (E). See also Movies S3 and S4.



Activated Bud1/Rsr1

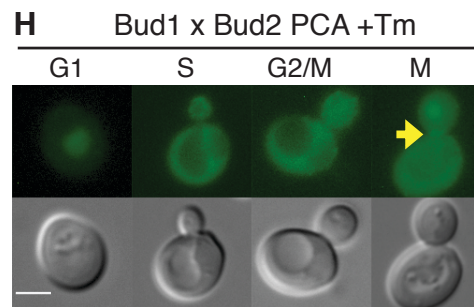
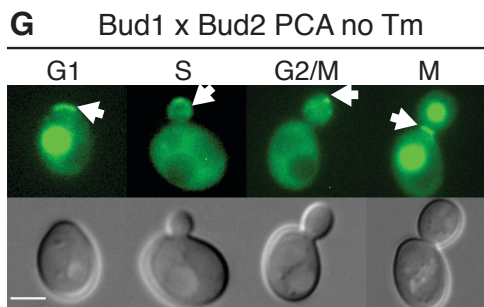
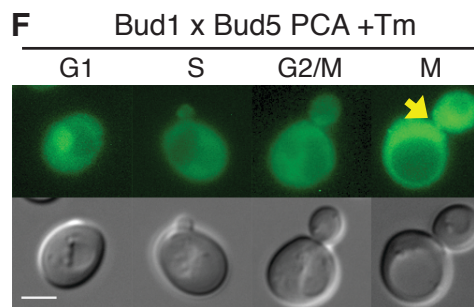
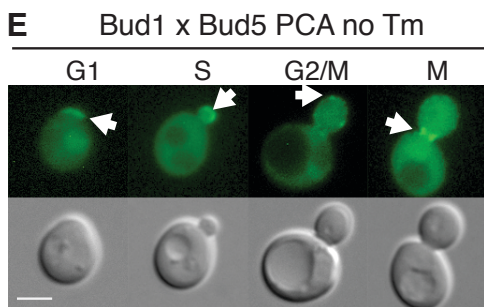
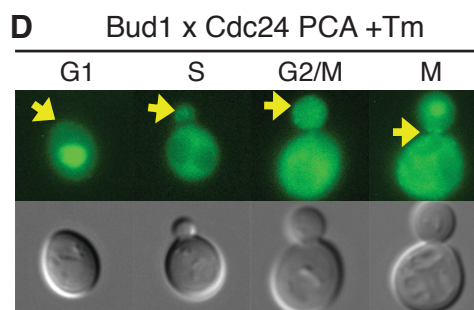
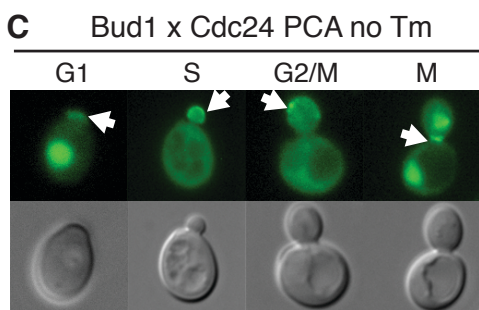


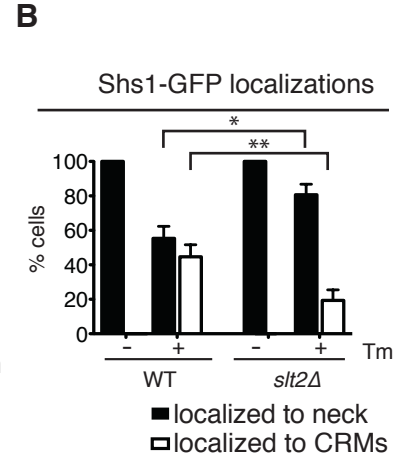
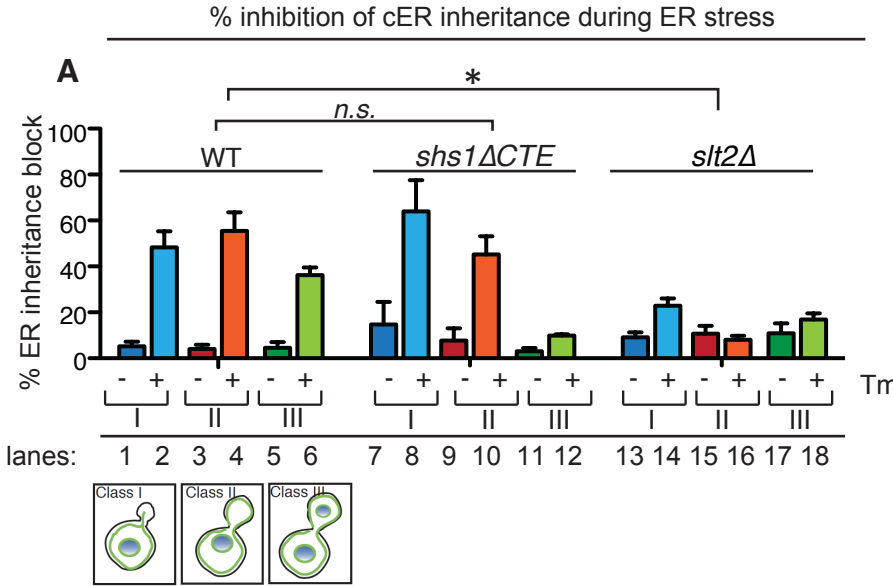
**Figure S2. Cdc42 is inactivated in response to ER stress induction (Related to Figure 2)**

(A-B) Time-lapse analysis of active Cdc42 (Gic2-PBD-RFP) in WT cells with or without 1 µg/ml Tm. See also Movies S5 and S6.

(C-D) Split-YFP PCA between Bud1 and Cdc24. Representative cells from each stage of the cell cycle are shown. Cells were grown with or without 1 µg/ml Tm. White arrows in untreated cells (C) indicate sites where Bud1 interacted with Cdc24 and a yellow arrows in (D) shows a small amount of Bud1 interaction with Cdc24 in ER-stressed cells.

(E-F) Split-YFP PCA between Bud1 and Bud5. Cells were grown with or without 1 µg/ml Tm. White arrows show where Bud1 and Bud5 interacted in untreated cells (E) and a yellow arrow in (F) shows a small amount of Bud1 interaction with Bud5 in ER stressed cells.

(G-H) Split-YFP PCA between Bud1 and Bud2. Cells were grown without (G) or with 1 µg/ml Tm (H). Bud1 and Bud2 interacted in unstressed cells (white arrows), and very little interaction (yellow arrow) was detected during ER stress in an M phase cell.



No change in Active CDC42 (Gic2) under ER stress

No change in CDC24 localization upon ER stress induction

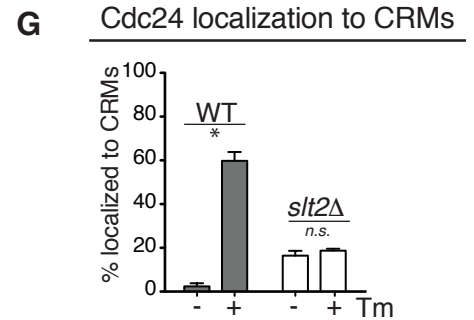
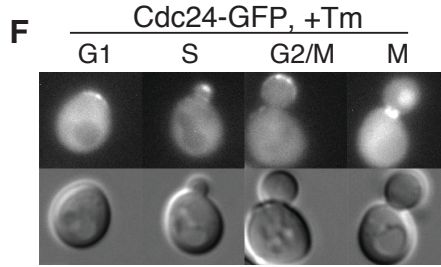
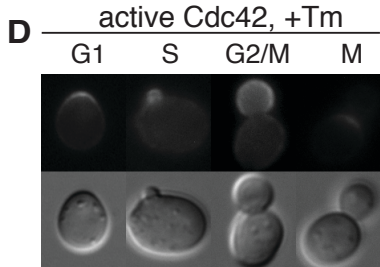
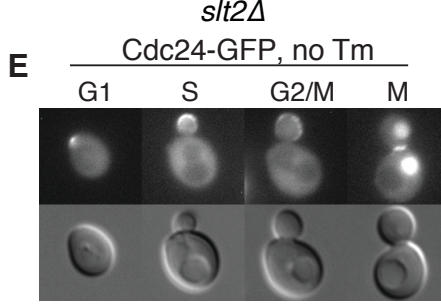
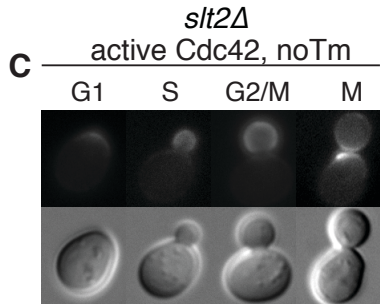


**Figure S3. *slt2Δ* cells fail to induce the ERSU pathway also fail to change in Cdc24 localization upon ER stress induction (Related to Figure 3)**

- (A) cER inheritance block in ER-stressed *shs1ΔCTE* and *slt2Δ* cells. The criteria for classes of cells used are as previously described (Babour et al., 2010): Class I represents cells with small buds of less than 2μm in diameter; Class II cells are cells with medium-large sized buds of 2 μm or larger; and class III are cells with large buds containing the inherited nucleus. Interestingly, the cER inheritance of ER-stressed class III *shs1ΔCTE* cells was not significantly affected. No significant level of the cER inheritance block occurred in ER-stressed *slt2Δ* cells. Two-way ANOVA comparing different strains' responses to ER stress showed that *shs1ΔCTE* was not significantly different than WT (n.s.), but *slt2Δ* was (\* represents  $p < 0.0001$ ).
- (B) Quantifications for Shs1-GFP localizations in WT and *slt2Δ* cells either untreated (-Tm) or treated with 1 μg/ml Tm (+Tm). \*,  $p < 0.05$ ; \*\*,  $p < 0.01$ .
- (C-D) Gic2-PBD-RFP in *slt2Δ* cells remained unchanged between untreated (C) and 1μg/ml Tm-treated (D) conditions.
- (E-F) Cdc24-GFP in *slt2Δ* cells remained unchanged between untreated (E) and 1μg/ml Tm-treated (F) conditions.
- (G) Quantification for Cdc24-GFP localized to CRMs in WT and *slt2Δ* cells with or without ER stress with Tm treatment (1μg/ml). T-tests comparing treated and untreated conditions showed that \* =  $p < 0.001$  and n.s. = not significant.

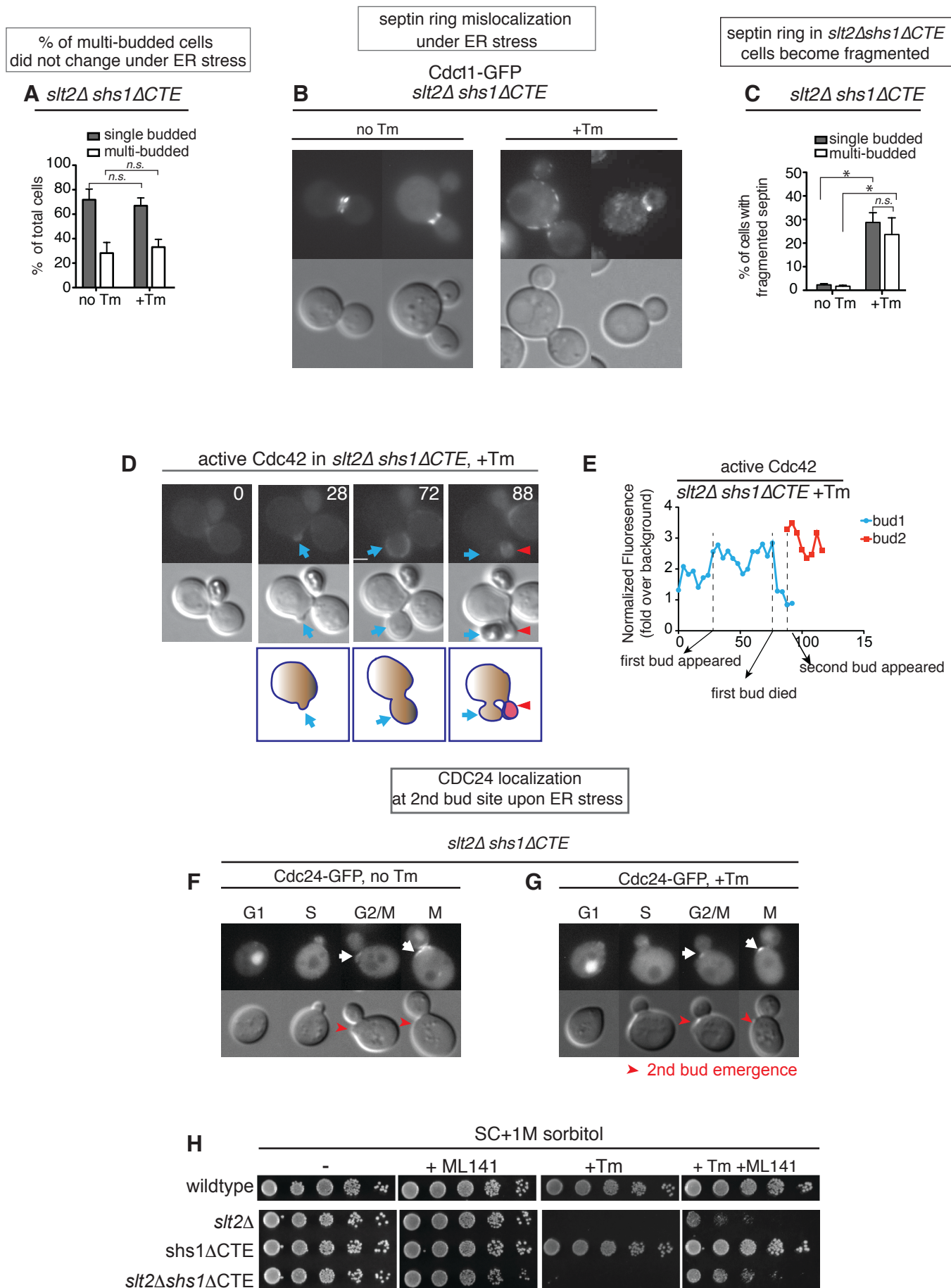


**Figure S4. Cdc42 is inactivated by Slt2 in *Shs1* $\Delta$ CTE cells** (Related to Figure 3)

(A) Some *slt2* $\Delta$  *shs1* $\Delta$ CTE cells were multi-budded even under normal growth without Tm. % of single and double budded cells between no Tm and +Tm were not significantly different (n.s).

(B-C) Cdc11-GFP was localized at the bud neck of single-budded *slt2* $\Delta$  *shs1* $\Delta$ CTE cells under normal growth conditions, but remained at the bud neck and did not translocate to CRMs upon ER stress induction (+Tm). In multi-budded *slt2* $\Delta$  *shs1* $\Delta$ CTE cells, Cdc11-GFP was localized only at one bud neck without ER stress, and it was mislocalized in the presence of Tm. (C) Quantitation showed that septin ring fragmentation was increased in ER stressed both single-budded and multi-budded *slt2* $\Delta$  *shs1* $\Delta$ CTE cells. \*represents  $p < 0.001$  and ns., not significant.

(D-E) Time-lapse analysis of active Cdc42 (Gic2-GFP) in the first and second buds emerged upon addition of Tm to *slt2* $\Delta$  *shs1* $\Delta$ CTE cells (time 0). Images from the time-lapse analysis taken at 0, 28, 72, and 88 sec are shown. Blue arrows show the first bud and red arrowheads show the second bud emerged from the original mother *slt2* $\Delta$  *shs1* $\Delta$ CTE cells. Quantification of Gic2-GFP fluorescence levels in the first (blue) bud and the second (red) bud at indicated times is in (D). See also Movie S7.

(F-G) Cdc24-GFP (white arrows) in *slt2* $\Delta$  *shs1* $\Delta$ CTE cells was localized to the incipient 2<sup>nd</sup> bud site (red arrowheads) under both normal growth or upon ER stress by treatment with Tm.

(H) Inactivation of Cdc42 rescued ER-stressed *slt2* $\Delta$  and *slt2* $\Delta$  *shs1* $\Delta$ CTE cells. A tenfold dilution of WT, *slt2* $\Delta$ , *shs1* $\Delta$ CTE, and *slt2* $\Delta$  *shs1* $\Delta$ CTE cells were spotted on synthetic complete medium with no Tm, 20 $\mu$ M ML141, +0.5  $\mu$ g/ml Tm or +(0.5

$\mu\text{g/ml Tm} + 20\mu\text{M ML141}$ ). ML141 is a well-characterized Cdc42 inactivating agent (Surviladze et al. 2010). As Slt2 is known to be involved in the cell wall integrity response (Verna et al., 1997), 1M sorbitol was added to suppress the cell wall integrity response.

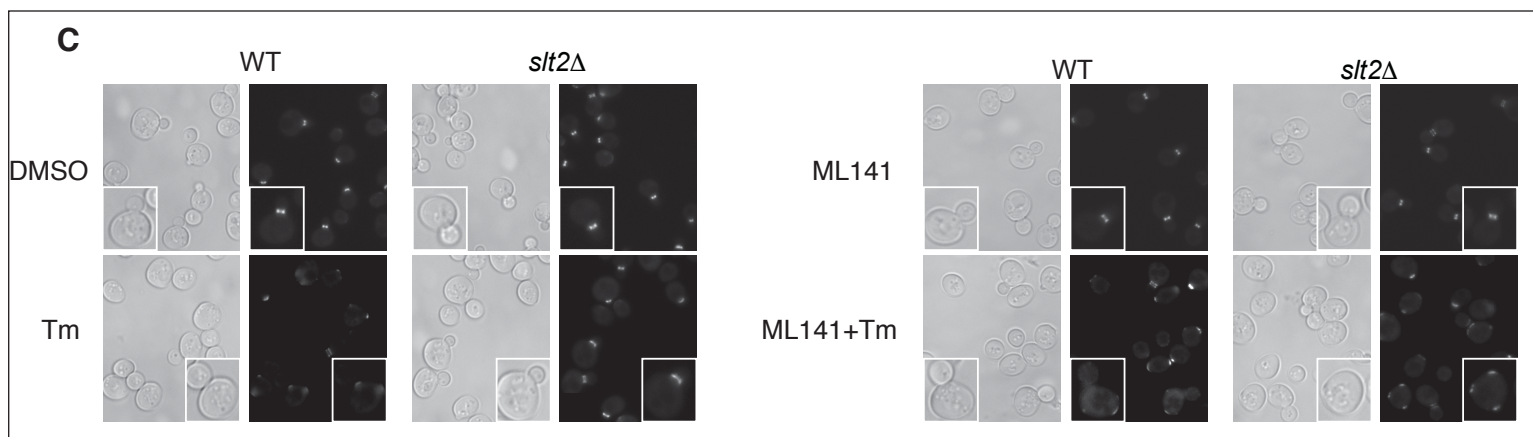
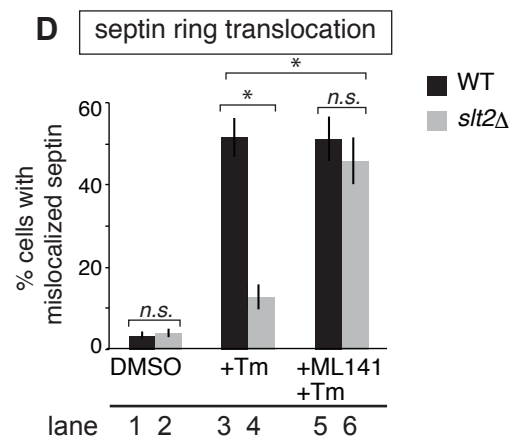
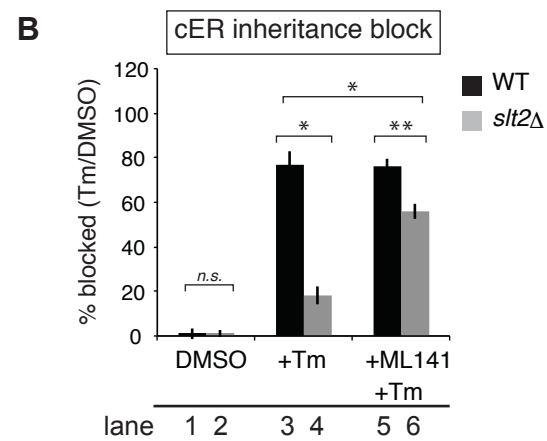
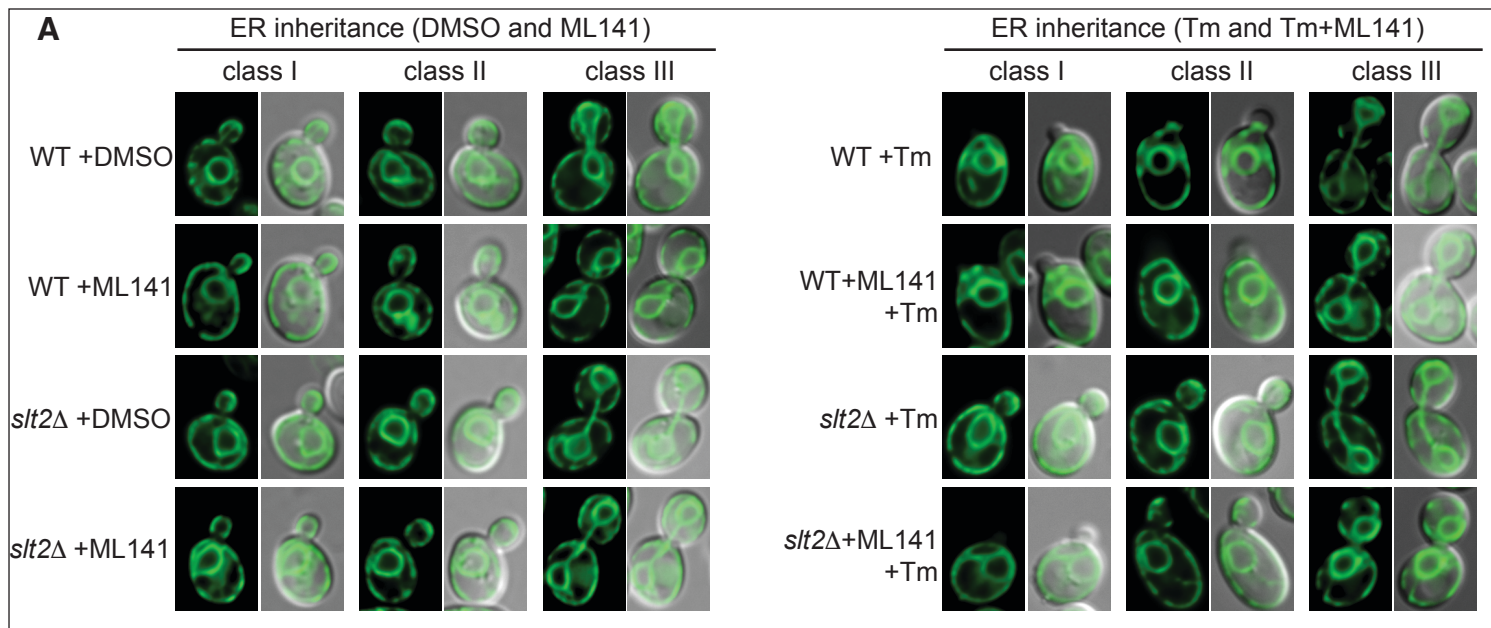


**Figure S5. *slt2Δ* cells fail to induce the ERSU pathway but can be rescued by a Cdc42 inhibitor** (Related to Figure 4)

- (A) Representative images of Shs1-GFP in WT and *slt2Δ* cells treated with DMSO, Tm (0.5 μg/ml), ML141 (20μM), or ML141 (20μM) plus Tm (0.5 μg/ml).
- (B) Quantification of the experiment is shown in (A). cER inheritance block of the ER-stressed *slt2Δ* cells (lane 4) was restored upon treatment with ML141 (lane 6). n.s., not significant; \*,  $p < 0.01$  ; \*\*,  $p < 0.05$ .
- (C) Representative images of septin ring localizations in WT and *slt2Δ* cells, treated similarly to (A) with the indicated compounds.
- (D) Quantifications of the experiment in (C). The septin ring failed to translocate in ER stress-induced ERSU-deficient *slt2Δ* cells (lane 4), and ML141 treatment of ER-stressed *slt2Δ* cells restored septin ring translocation to CRMs (lane 6).

Figure S6

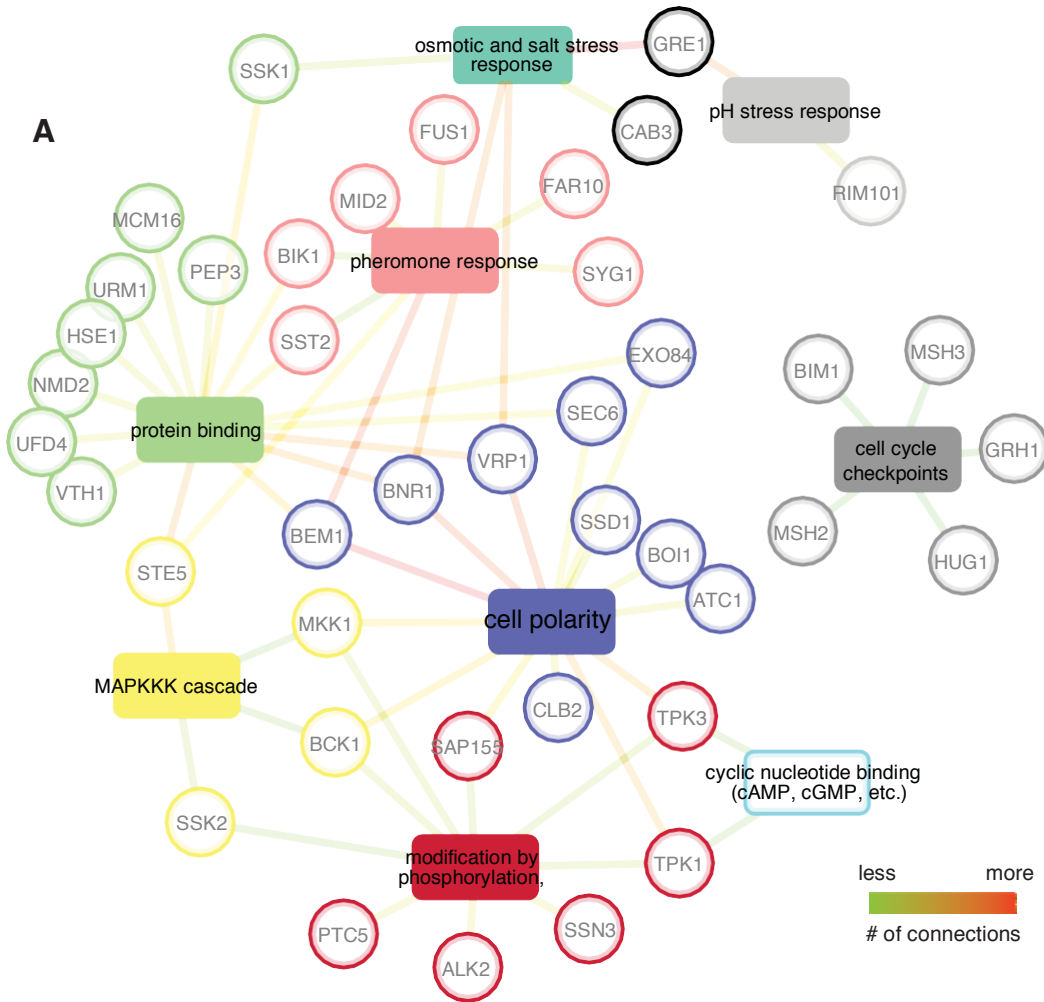


**Figure S6. Identification of Bem1 as a Slr2-interacting protein (Related to Figure 4)**

- (A) Functional interaction map for Slr2 derived from protein-protein interactions identified in the split-DHFR screen. Nodes represent functional categories, and edges define associations with Slr2. Edge length and thickness indicate fold enrichment, which is defined as the number of proteins from the input dataset relative to the total number of proteins in a given category. For details on the analysis, see Materials and Methods. See also Table S1-3.

## Supplemental Table

Table S1. Top 100 Slt2 interactors from the DHFR screen, Related to Figure 5

**Table S1: Sit2 Interactors during stress by DHFR protein complementation assay**

ORF Name	Protein Name	SGD Description	Area- <i>DTT</i> (M)		Area+ <i>DTT</i> (M)		Ratios (+/-)		Fold increase	Abundance	Interaction score
			Area- <i>DTT</i> (M)	Area+ <i>DTT</i> (M)	Area- <i>DTT</i> (M)	Area+ <i>DTT</i> (M)	Ratios (+/-)	Ratios (+/-)			
YBR165W	UBS1	Ubiquitin-conjugating enzyme suppressor that	63	61	1.0	55	76	1.4	1.2	0	#DIV/0!
YBR186W	PCH2	Hexameric ring ATPase that remodels chromo	48	52	1.1	53	58	1.1	1.1	0	#DIV/0!
YNL128W	TEP1	PTEN homolog with no demonstrated inositol	62	68	1.1	51	54	1.1	1.1	0	#DIV/0!
YGL143C	MRF1	Mitochondrial translation release factor; invol	39	54	1.4	289	308	1.1	1.2	960	18.8453881
YFR029W	PTR3	Component of the SPS plasma membrane ami	53	50	0.9	88	130	1.5	1.2	499	18.0257192
YPL008W	CHL1	Probable DNA helicase; involved in sister-chro	54	60	1.1	52	62	1.2	1.2	395	15.4287502
YBR270C	BIT2	Subunit of TORC2 membrane-associated comp	52	68	1.3	52	69	1.3	1.3	572	11.9761483
YGR057C	LST7	Subunit of the Lst4p-Lst7p GTPase activating p	58	67	1.2	95	153	1.6	1.4	932	11.8085422
YPR119W	CLB2	B-type cyclin involved in cell cycle progression	62	63	1.0	51	64	1.3	1.1	569	11.1579631
YKL132C	RMA1	Putative dihydrofolate synthetase; similar to E	54	52	1.0	76	117	1.5	1.3	787	10.7369759
YBL009W	ALK2	Protein kinase; along with its paralog, ALK1, re	71	66	0.9	53	67	1.3	1.1	626	10.6177748
YBL005W	PDR3	Transcriptional activator of the pleiotropic dru	54	59	1.1	51	57	1.1	1.1	583	9.94866321
YFL046W	FMP32	Putative assembly factor for cytochrome c oxi	51	84	1.6	55	95	1.7	1.7	920	9.72342043
YLR425W	TUS1	Guanine nucleotide exchange factor (GEF) tha	54	60	1.1	51	54	1.1	1.1	630	9.04921728
YBR239C	ERT1	Transcriptional regulator; involved in regulatio	56	103	1.8	65	96	1.5	1.7	1100	9.04248805
YDR184C	ATC1	Nuclear protein; possibly involved in regulatio	82	79	1.0	52	72	1.4	1.2	881	8.56558955
YLR238W	FAR10	Protein involved in recovery from arrest in res	55	60	1.1	51	52	1.0	1.1	669	8.37463775
YHR134W	WSS1	SUMO-ligase and SUMO-targeted metalloprot	53	63	1.2	101	123	1.2	1.2	1168	7.9589657
YJL095W	BCK1	MAPKKK acting in the protein kinase C signalin	63	77	1.2	59	71	1.2	1.2	1007	7.34929726
YML058W-A	HUG1	Ribonucleotide reductase inhibitor; intrinsicall	80	117	1.5	158	216	1.4	1.4	2339	7.11699466
YJR127C	RSF2	Zinc-finger protein; involved in transcriptional	44	67	1.5	55	61	1.1	1.3	929	6.88717709
YDL245C	HXT15	Putative transmembrane polyol transporter; s	64	72	1.1	71	110	1.5	1.3	1370	6.64152099
YPL072W	UBP16	Deubiquitinating enzyme anchored to the out	62	74	1.2	64	97	1.5	1.4	1306	6.5491598
YPL003W	ULA1	Protein that activates Rub1p (NEDD8) before n	58	72	1.2	54	78	1.4	1.3	1174	6.39041147
YOR231W	MKK1	MAPKK involved in the protein kinase C signali	69	76	1.1	63	72	1.1	1.1	1185	6.24406516
YOR077W	RTS2	Basic zinc-finger protein; similar to human and	111	96	0.9	90	157	1.7	1.3	2035	6.2170095
YNR031C	SSK2	MAP kinase kinase kinase of HOG1 mitogen-ac	48	72	1.5	63	76	1.2	1.4	1207	6.13082056
YLR204W	QRI5	Mitochondrial inner membrane protein; requi	49	45	0.9	57	97	1.7	1.3	1275	5.56952869
YIL173W	VTH1	Putative membrane glycoprotein; has strong s	59	53	0.9	62	90	1.5	1.2	1310	5.45798542
YDL139C	SCM3	Nonhistone component of centromeric chrom	58	52	0.9	53	71	1.3	1.1	1130	5.44207996
YOL103W	ITR2	Myo-inositol transporter; member of the suga	51	63	1.2	58	85	1.5	1.4	1393	5.31274873
YPL171C	OYE3	Conserved NADPH oxidoreductase containing	60	51	0.9	151	196	1.3	1.1	2340	5.27824037
YPR046W	MCM16	Component of the Ctf19 complex and the COM	59	57	1.0	53	63	1.2	1.1	1159	5.17581014
YOR350C	MNE1	Protein involved in splicing Group I al5-beta in	54	63	1.2	56	85	1.5	1.3	1441	5.13362599
YLR037C	PAU23	Cell wall mannoprotein; has similarity to Tir1p	51	57	1.1	51	69	1.4	1.2	1241	5.07715835
YIR002C	MPH1	3'-5' DNA helicase involved in error-free bypas	47	56	1.2	56	60	1.1	1.1	1168	4.96624473
YJR152W	DAL5	Allantoate permease; ureidosuccinate permea	51	50	1.0	74	107	1.4	1.2	1617	4.85526896
YML042W	CAT2	Carnitine acetyl-CoA transferase; present in bo	48	61	1.3	57	81	1.4	1.3	1474	4.81684304
YDL189W	RBS1	Protein involved in assembly of the RNA polym	54	52	1.0	111	175	1.6	1.3	2393	4.74261264
YDR103W	STE5	Pheromone-responsive MAPK scaffold protein	45	72	1.6	51	60	1.2	1.4	1482	4.45207867

(colony size in *DTT*/Abundance)

YHL027W	RIM101	Cys2His2 zinc-finger transcriptional repressor;	55	62	1.1	53	60	1.1	1.1	1397	4.36666936
YCR067C	SED4	Integral ER membrane protein that stimulates	56	59	1.1	61	72	1.2	1.1	1502	4.36124359
YCR092C	MSH3	Mismatch repair protein; forms dimers with M	57	70	1.2	51	57	1.1	1.2	1459	4.35132753
YOL028C	YAP7	Putative basic leucine zipper (bZIP) transcripti	50	66	1.3	51	61	1.2	1.3	1472	4.31508179
YDR316W	OMS1	Protein integral to the mitochondrial membra	53	47	0.9	74	102	1.4	1.1	1825	4.08197866
YLR148W	PEP3	Component of CORVET membrane tethering c	53	94	1.8	51	77	1.5	1.6	2306	3.70749321
YDR482C	CWC21	Protein involved in RNA splicing by the spliceo	52	50	1.0	69	109	1.6	1.3	2220	3.58135739
YOR054C	VHS3	Negative regulatory subunit of protein phosph	53	63	1.2	52	81	1.6	1.4	2059	3.49611199
YLR006C	SSK1	Cytoplasmic phosphorelay intermediate osmo	54	79	1.5	63	68	1.1	1.3	2127	3.45580877
YDR108W	GSG1	Component of transport protein particle (TRA	51	60	1.2	51	63	1.2	1.2	1822	3.37535534
YBR246W	RRT2	Methylesterase performing penultimate step	67	68	1.0	53	68	1.3	1.1	2076	3.27509321
YCL029C	BIK1	Microtubule-associated protein; component o	56	63	1.1	59	63	1.1	1.1	1927	3.26967443
YLR119W	SRN2	Component of the ESCRT-I complex; ESCRT-I is	52	44	0.8	54	87	1.6	1.2	2007	3.26432062
YIL068C	SEC6	Essential 88kDa subunit of the exocyst comple	55	63	1.1	62	70	1.1	1.1	2100	3.16591611
YDL106C	PHO2	Homeobox transcription factor; regulatory tar	66	89	1.3	52	67	1.3	1.3	2481	3.14440962
YKL086W	SRX1	Sulfiredoxin; contributes to oxidative stress re	47	66	1.4	51	53	1.0	1.2	1916	3.10597984
YHR059W	FYV4	Protein of unknown function; required for sur	55	65	1.2	62	87	1.4	1.3	2469	3.07762613
YNL309W	STB1	Protein with role in regulation of MBF-specific	48	68	1.4	56	61	1.1	1.3	2150	2.99969797
YIL150C	MCM10	Essential chromatin-associated protein; involv	53	62	1.2	57	65	1.1	1.2	2142	2.96472319
YPL042C	SSN3	Cyclin-dependent protein kinase; component	65	78	1.2	57	62	1.1	1.1	2399	2.91752657
YIL047C	SYG1	Plasma membrane protein of unknown functio	55	68	1.2	57	62	1.1	1.2	2277	2.85468386
YLR085C	ARP6	Actin-related protein that binds nucleosomes;	71	72	1.0	60	67	1.1	1.1	2438	2.8508181
YDR257C	RKM4	Ribosomal lysine methyltransferase; specific f	50	49	1.0	122	158	1.3	1.1	3631	2.85048507
YBR102C	EXO84	Exocyst subunit with dual roles in exocytosis a	42	76	1.8	54	55	1.0	1.4	2306	2.84011649
YAL055W	PEX22	Putative peroxisomal membrane protein; requ	52	44	0.8	82	116	1.4	1.1	2824	2.83332625
YBR216C	YBP1	Protein involved in cellular response to oxidati	43	53	1.2	53	64	1.2	1.2	2120	2.75929796
YHR077C	NMD2	Protein involved in the nonsense-mediated m	43	61	1.4	51	53	1.0	1.2	2172	2.62455025
YIL066C	RNR3	Minor isoform of large subunit of ribonucleoti	45	59	1.3	79	120	1.5	1.4	3439	2.60237945
YKL088W	CAB3	Subunit of PPCDC and CoA-SPC complexes inv	58	73	1.3	59	85	1.4	1.3	3121	2.53146011
YCL027W	FUS1	Membrane protein localized to the shmoo tip;	57	62	1.1	54	58	1.1	1.1	2383	2.51776697
YER016W	BIM1	Microtubule plus end-tracking protein; togeth	57	67	1.2	65	70	1.1	1.1	2782	2.46193309
YIL159W	BNR1	Formin; nucleates the formation of linear actin	49	56	1.1	62	81	1.3	1.2	2855	2.39947693
YJR022W	LSM8	Lsm (Like Sm) protein; forms heteroheptameri	57	65	1.1	53	59	1.1	1.1	2626	2.36130922
YLR337C	VRP1	Verprolin, proline-rich actin-associated protein	66	82	1.2	64	86	1.3	1.3	3559	2.36020717
YLR332W	MID2	O-glycosylated plasma membrane protein; act	67	59	0.9	84	115	1.4	1.1	3816	2.27986762
YDR527W	RBA50	Protein involved in transcription; interacts wit	55	50	0.9	55	92	1.7	1.3	3119	2.27628146
YPR040W	TIP41	Protein that interacts with Tap42p, which regu	59	70	1.2	54	55	1.0	1.1	2857	2.18795926
YKL010C	UFD4	Ubiquitin-protein ligase (E3); interacts with Rp	66	80	1.2	54	75	1.4	1.3	3564	2.17450404
YGL023C	PIB2	Protein of unknown function; contains FYVE d	63	67	1.1	52	64	1.2	1.1	3043	2.1523572
YIL008W	URM1	Ubiquitin-like protein involved in thiolation of	64	85	1.3	58	87	1.5	1.4	4001	2.14936442
YOL090W	MSH2	Protein that binds to DNA mismatches; forms	54	63	1.2	56	80	1.4	1.3	3467	2.06246036
YMR076C	PDS5	Cohesion maintenance factor; involved in siste	51	59	1.2	76	84	1.1	1.1	3468	2.06143603

YJL164C	TPK1	cAMP-dependent protein kinase catalytic subu	56	76	1.4	63	74	1.2	1.3	3704	2.02500528
YOR090C	PTC5	Mitochondrial type 2C protein phosphatase (P	52	52	1.0	72	122	1.7	1.3	4366	1.99267873
<b>YBR200W</b>	<b>BEM1</b>	<b>Protein containing SH3-domains; involv</b>	<b>57</b>	<b>66</b>	<b>1.2</b>	<b>45</b>	<b>52</b>	<b>1.2</b>	<b>1.2</b>	2994	1.97053231
YPL099C	AIM43	F1F0 ATPase synthase peripheral stalk assemb	20	19	1.0	51	64	1.3	1.1	2130	1.9481147
YBL085W	BOI1	Protein implicated in polar growth; functionall	57	64	1.1	51	60	1.2	1.1	3220	1.92567763
YFR040W	SAP155	Protein required for function of the Sit4p prot	56	62	1.1	60	74	1.2	1.2	3591	1.8938715
YBL102W	SFT2	Tetra-spanning membrane protein found mos	69	73	1.1	64	81	1.3	1.2	4102	1.87714853
YKL166C	TPK3	cAMP-dependent protein kinase catalytic subu	56	78	1.4	51	55	1.1	1.2	3574	1.86051943
YHL002W	HSE1	Subunit of the endosomal Vps27p-Hse1p com	57	60	1.1	51	56	1.1	1.1	3141	1.8466628
YDR293C	SSD1	Translational repressor with a role in polar gro	57	115	2.0	154	185	1.2	1.6	8160	1.83816239
YPL223C	GRE1	Hydrophilin essential in desiccation-rehydratio	59	70	1.2	56	58	1.0	1.1	3491	1.83306162
YHR199C	AIM46	Protein of unknown function; the authentic, n	65	69	1.1	51	64	1.3	1.2	3638	1.82774593
YMR292W	GOT1	Homodimeric protein that is packaged into CO	63	69	1.1	51	60	1.2	1.1	3615	1.78416597
YMR093W	UTP15	Nucleolar protein; component of the small sub	52	65	1.3	53	97	1.8	1.5	4549	1.78060621
YLR452C	SST2	GTPase-activating protein for Gpa1p; regulate	58	64	1.1	51	52	1.0	1.1	3419	1.69626181
YDR517W	GRH1	Acetylated cis-Golgi protein, homolog of huma	43	60	1.4	58	84	1.4	1.4	4365	1.64951384
YDL088C	ASM4	FG-nucleoporin component of central core of	61	74	1.2	51	53	1.0	1.1	3940	1.61152272

Table S2. Results of GO analysis of top 100 Slt2 interactors, Related to Figure 5

**Table S2: GO Analysis of Top 100 DHFR hits by MIPS Functional Classification (459 categories) (Related to Figure 5)**

Category	p-value	In Category from Cluster	k	f
protein binding [16.01]	0.0002031	EXO84 BEM1 BIK1 STE5 HSE1 NMD2 URM1 SEC6 BNR1 VTH1 UFD4 SSK1 PEP3 VRP1 SST2 MCM16	16	391
budding, cell polarity and filament formation [43.01.03.05]	0.0002056	BOI1 EXO84 BEM1 ATC1 SSD1 SAP155 SEC6 BNR1 BCK1 TPK1 TPK3 VRP1 MKK1 CLB2	14	312
MAPKKK cascade [30.01.05.01.03]	0.0006403	STE5 BCK1 SSK2 MKK1	4	27
cyclic nucleotide binding (cAMP, cGMP, etc.) [16.19.01]	0.001309	TPK1 TPK3	2	4
modification by phosphorylation, dephosphorylation, autophosphorylation [14.07.03]	0.001794	ALK2 SAP155 BCK1 TPK1 TPK3 SSK2 PTC5 MKK1 SSN3	9	186
osmotic and salt stress response [32.01.03]	0.001806	BNR1 CAB3 SSK1 VRP1 GRE1	5	59
cell cycle checkpoints (checkpoints of morphogenesis, DNA-damage,-replication, mitotic phase and spindle) [10.03.01.03]	0.003171	MSH3 GRH1 BIM1 HUG1 MSH2	5	67
pH stress response [32.01.04]	0.005875	RIM101 GRE1	2	8
pheromone response, mating-type determination, sex-specific proteins [34.11.03.07]	0.007208	BEM1 FUS1 BIK1 STE5 SYG1 FAR10 MID2 SST2	8	189

**Supplemental Information**

**Supplemental Video**

Video S1. Shs1-GFP translocation in an untreated WT cell. Related to Figure 1A.

Video S2. Shs1-GFP translocation during ER stress in a WT cell. Related to Figure 1B.

Video S3. Shs1-GFP translocation in an untreated WT cell of the W303 background.

Related to Figure 1D.

Video S4. Shs1-GFP translocation in W303 WT cell during ER stress. Related to Figure S1E.

Video S5. Dynamics of active Cdc42 in an untreated WT cell. Related to Figure S2A.

Video S6. Dynamics of active Cdc42 during ER stress. Related to Figure S2A.

Video S7. Dynamics of active Cdc42 in ER-stressed *slt2Δ shs1CTE* double mutant.

Related to Figure 5

Video S8. Shs1-GFP dynamics in a WT cell that was first treated with Tm and then washed into normal medium for recovery. Related to Figure 6B-C.

Video S9. Dynamics of active Cdc42 during recovery from ER stress. Related to Figure

6E.

Video S10. Shs1 $\Delta$ CTE-GFP dynamics during recovery from ER stress. Related to Figure

6F-G.

Video S11. Shs1-GFP dynamics in a *bem1* $\Delta$  cell during recovery from ER stress. Related to Figure 6H-I.

Video S12. Shs1-GFP dynamics in an aged cell during recovery from ER stress. Related to Figure 7F-G